DIAGNOSTIC STUDIES AND ANALYTICAL CHARACTERISTICS OF A HIGH POWER HELIUM/HYDROGEN CAPACITIVELY COUPLED MICROWAVE PLASMA

By

WELLINGTON R.L. MASAMBA

A DISSERTATION PRESENTED TO THE GRADUATE SCHOOL
OF THE UNIVERSITY OF FLORIDA IN PARTIAL FULFILLMENT
OF THE REQUIREMENTS FOR THE DEGREE OF
DOCTOR OF PHILOSOPHY

UNIVERSITY OF FLORIDA

1992

Dedicated to my mother and father for their
love, support, and sacrifices.

ACKNOWLEDGEMENTS

I would like to express my sincere gratitude to my research advisor, Professor James D. Winefordner, for his exceptional patience throughout the course of this work. He believed in me even during times when he had reasons to believe otherwise. His financial support is also gratefully acknowledged.

Many of Winefordner's group members made this work a lot easier than it would otherwise have been. I am grateful to Ben Smith to whom I turned for answers to most of my questions ranging from those of a technical nature to location of equipment. Dennis Hueber cheerfully and humorously helped with computers. Most of the data in this work was processed by the SIDE program written by him. Collaboration with Dennis on Chapter four is also acknowledged. For their friendship and support, I am indebted to Giuseppe Petrucci, who together with Ben, rekindled my interest in racquetball, Nancy Petrucci, Edison Becerra, Jim Deavor, MaryAnn Gunshefski, Cheri Morgan, Donna Robie, Yuan-Hsiang Lee, Chonyu Chen, Denise Imbroisi, Wilfredo Resto, and Nancy Mullins, just to mention a few.

My thanks also go to the glass shop for construction of the quartz torch, and the machine shop for making the electrodes used in this work.

I would also like to thank the Malawi Government for providing airfare and supplementing my assistantship.

My deepest love and gratitude go to my family, who never faltered in their support. This work would not have been possible without the love of my parents, and my brothers, Chris and Sam. I hope that this work will inspire the rest of my brothers and sisters to fight for excellence in whatever they choose to do. Because of this work, my nieces have missed my presence for more than 60% of their lives. Chisomo was born when I was doing my studies and left Malawi for the United Kingdom with her parents before I returned. We met at the airport for the first time when she was over four years old! I returned to the U.S. to complete my studies three months later, missing the birth of Lisungu, her young sister, by a few days. I have missed Chimwemwe's first and second birthdays.

Finally, but definitely not of least importance, I would like to thank my wife to be, Jeyna, for her patience and understanding. Even though she was thousands of miles away, her love and encouragement is appreciated probably more than she will ever know.

TABLE OF CONTENTS

PAGE

ACKNOWLEDGEMENTS....................iii

ABSTRACT....................viii

CHAPTERS

1 CAPACITIVELY COUPLED MICROWAVE PLASMAS....................1

- Introduction....................1
- History....................3
- Applications....................5
- Instrumentation....................6
  - Microwave Power Sources....................9
  - Waveguides....................9
  - Coupling Power into and out of Waveguides....................12
  - Instrumentation Used in this Work....................12
  - The Plasma....................27

2 DIAGNOSTIC STUDIES....................33

- Introduction....................33
- Theory....................34
  - Electronic Excitation Temperature....................34
  - Rotational Temperature from Band Systems of Diatomic Molecules....36
  - Electron Number Densities....................38
- Experimental....................39
  - Measurement of Electronic Excitation Temperature....................40
  - Measurement of Rotational Temperature....................40
  - Electron Number Density Determinations....................46
- Results and Discussion....................46
  - Effect of Radial Position....................46
  - Effect of Axial Position....................51
  - Effect of Carrier Gas....................56
  - Effect of Solution Uptake Rate....................61
  - Effect of Power....................61
- Summary....................70

3 EFFECT OF HYDROGEN ON PLASMA CHARACTERISTICS.....72

Introduction.....72
Experimental.....74
Results and Discussion.....75
  Electronic Excitation Temperature.....75
  Rotational Temperature.....75
  Electron Number Density.....78
  Effect on Emission Signals.....78
Summary.....90

4 ANALYSIS OF ARSENIC AFTER HYDRIDE GENERATION....91

Introduction.....91
Experimental.....94
  Reagents.....95
  Procedure for Measurement.....95
Results and Discussion.....98
  Optimum heating rate of the AsH_3 trap.......103
  Effect of Power.....108
  Limit of Detection and Linear Dynamic Range.....108
Summary.....108

5 ANALYSIS BY SOLUTION NEBULIZATION.....114

Introduction.....114
Experimental.....115
Results and Discussion.....115
  Effect of Various Parameters on Cr Emission.....115
  Effect of Power.....119
  Limits of Detection.....119
  Matrix Interferences.....127
Summary.....129

6 ANALYSIS OF STEEL BY DIRECT SAMPLE INJECTION...134

Introduction.....134
Experimental.....136
Results and Discussion.....136
Summary.....150

7 CONCLUSIONS AND FUTURE WORK.....151

APPENDIX SPECTRA OF SOME ELEMENTS OBTAINED BY SOLUTION NEBULIZATION......................158

REFERENCES...161

BIOGRAPHICAL SKETCH......................................170

Abstract of Dissertation Presented to the Graduate School
of the University of Florida in Partial Fulfillment of the
Requirements for the Degree of Doctor of Philosophy

DIAGNOSTIC STUDIES AND ANALYTICAL CHARACTERISTICS OF A HIGH POWER HELIUM/HYDROGEN CAPACITIVELY COUPLED MICROWAVE PLASMA

By

Wellington R.L. Masamba

August 1992

Chairperson: James D. Winefordner
Major Department: Chemistry

Microwave plasmas have advantages over other plasma systems in that they have low initial and operational costs. Most work on microwave plasmas has been with systems operating at low to medium powers, resulting in problems with sample introduction and severe matrix interferences.

This work describes the construction of a high power capacitively coupled microwave plasma (up to 1.6 kW) employing a graphite electrode. A mixture of helium and hydrogen was used as the plasma gas. Several important diagnostic parameters (electronic excitation temperature, rotational temperature, and electron number densities) were determined under different plasma conditions. The plasma was also used to analyze gas, solution, and solid samples.

Depending on plasma conditions, electronic excitation temperatures were determined to lie between 2000 K and 5000 K, rotational temperatures were between 1800 K and 3000 K, and electron number densities varied between $4x10^{14}$ cm^{-3} and $9x10^{14}$ cm^{-3}. The limit of detection for arsenic after hydride generation were determined to be 0.03 ng or 0.4 pg/mL if a 75 mL sample is used. Limits of detection determined by solution nebulization were in the sub part per million range. Very little interference of Na on Ca was observed, while slight depression of Ca signal by PO_4^{3-} was observed at PO_4^{3-} concentrations above 100 ppm. Direct introduction of metal samples into the plasma resulted in linear calibration curves with limits of detection of 0.08 and 5 µg/g for Pb and Sn, respectively.

CHAPTER 1
CAPACITIVELY COUPLED MICROWAVE PLASMAS

Introduction

Microwave plasmas are classified according to the means by which energy is transferred to the plasma into microwave induced plasma (MIP) and capacitively coupled microwave plasma (CMP) systems. An MIP is formed in a discharge tube placed in a cavity to which power is transmitted via a coaxial cable line [1]. In CMPs, a magnetron generates microwaves that are conducted through a waveguide to the tip of a single electrode, where a flame-like plasma is formed [2].

Compared to other plasma systems in optical emission spectroscopy (OES), such as the inductively coupled plasma optical emission spectroscopy (ICP-OES), microwave plasma optical emission spectroscopy has the advantages of lower initial and operational costs. Components used in microwave plasmas are of low cost. The popular use of microwave ovens has resulted in availability of low cost magnetrons capable of delivering medium to high powers. Most of the microwave plasmas operate at gas flow rates far less than those employed in ICPs, resulting in low operational cost. Although microwaves can cause injury, especially at high radiation levels, they can easily be contained within wire mesh or metal shields. Radio frequency (RF) shielding in ICPs has to be more elaborate. Whereas ICPs have mostly employed argon and, to a lesser extent, nitrogen as the plasma gases, microwave plasmas have been successfully generated using other gases, such as He and air as well. Most of the earlier microwave plasmas, however, were operated at low (<150 W) or medium (150-400 W) power levels resulting in low tolerance for molecular species introduced into the plasma as well as matrix effects. The potential for microwave plasmas has not been fully explored, probably as a result of the success of atomic absorption spectrometry (AAS) and lately ICP-OES.

MIPs show better stability and lower background noise (for OES) compared to CMPs operated at comparable power levels and do not suffer from possible contamination from electrode material. Also in CMPs the electrode needs to be replaced from time to time. Because of these reasons, most of the work on microwave plasmas has concentrated on MIPs as evident from reviews on the subject [3-9].

In spite of the drawbacks mentioned above for CMPs, they have distinct advantages over MIPs. CMPs can be formed over a wider power range. In MIPs, the coaxial cable feeding power to the cavity heats up and radiates microwaves as power is increased beyond 150 W [10]. Most MIPs are therefore designed to operate at low power levels with concomitant problems with introduction of molecular species into the plasma. MIPs were therefore initially used as detectors for gases [8], for gas chromatography (GC) [11,12] or simple, easily fragmented volatile compounds [13]. High power levels may be employed in CMPs by using waveguides as the means of transferring power to the plasma gas. Operation of CMPs at medium to high power levels results in more tolerance to introduction of molecular species such as water aerosols. CMPs can be sustained more easily than MIPs by a variety of gases such as He, Ar, N_2 and air. This work will only deal with CMPs, and MIPs will not be discussed further except for comparison purposes only.

History

Capacitively coupled plasmas (CCPs) have been generated at various frequencies in both the radio frequency (RF) and microwave regions of the electromagnetic spectrum. They were first described in 1941 by Gritescu and Grigorovici [14-16] who applied the output of a high frequency oscillator to two circular plates which were separated by a vertical distance of up to 15 cm. The lower plate had a copper cone with a platinum tip. The plates formed a capacitor which was part of a circuit determining the frequency of the oscillator, typically in the range 60-90 MHz. The discharge was formed at the tip by touching it with an isolated conductor. Analytical applications were reported for the first time by Stolov [17] and Badarau et al. [18].

A comprehensive history of CMPs is given by Dahmen [19,20]. Microwave discharges were first observed by physicists and electrical engineers as unwanted and disturbing effects in the development of RADAR equipment [21,22]. In 1951 a microwave torch discharge operated at 1000 MHz and used as a heating device was described by Cobine and Wilbur [23]. Using air, N_2, or CO_2 plasmas, they were able to show that the plasma could reach temperatures greater than 3370 °C by melting tungsten rods. Changing the plasma gas to 0.3% H_2 in He resulted in lower temperatures. In fact, a pure Ar plasma at 100 W could not ignite a piece of paper held axially in the plasma. A pure He plasma was also shown to be cool. They attributed these observations to the absence of dissociable species in the He and Ar plasmas and attributed the high temperature of the polyatomic plasmas to the heat of association of atoms dissociated from the molecules. A similar torch was introduced as an excitation source for spectrochemistry by Mavrodineanu and Hughes [24,25]. In 1963, Jecht and Kessler [26] published a paper on the excitation mechanisms of a CMP plasma similar to that of ref. [24]. Kessler and Gebhardt published a paper on analysis of limestone, [27] and later, Kessler published a paper on analysis of glasses [28]. Development of CMP centered about the work of Kessler and his coworkers [26-28] in Germany and work by Murayama, Yamamoto and Goto [29-34] in Japan. These various efforts resulted in CMP equipment commercialized [35] by (1) Hitachi, Tokyo Japan, designated "ultra high frequency (UHF) plasma," (2) Applied Research Laboratories, Ecublens-Lausanne, Switzerland, and (3) Erbe-Elektromedizin, Tuebingen, Germany.

Applications

Since the early applications of CMPs to analysis of real samples [27,28], several authors have reported other analytical applications. Govindaraju et al. [36] reported a method for the analysis of silicate rocks and minerals, after buffering with Sr and Li to eliminate matrix interferences, using a Kessler-type CMP with a Cu or Ag electrode, operated at 600 W. Burman and Bostrom [37] compared the performance of CMP and ICP for the analysis of geological material and concluded that the CMP suffered severely from matrix effects except in the presence of ionization buffers. No buffers were needed for analysis using the ICP. Larson and Fassel [38] and Boumans et al. [39] also indicated superior performance of the ICP compared to CMP, especially with respect to matrix interferences. In both cases the CMP was operated at 600 W while the ICP was operated at power levels greater than 1 kW.

Nakashima et al. [40] and Suzuki [41-43] reported CMP analysis of steel. Huang and Blades [44] and Hiroshi et al. [45] used CMP systems as a GC detector for organotin compounds, while Ali et al. [46] used direct solid sampling CMP atomic emission to determine elements in tomato leaves and coal fly ash. The powdered sample (sometimes diluted with graphite) was placed on the electrode shaped as a cup, and emission signals were obtained after drying and ashing stages accomplished by using low microwave power levels. Zhang et al. [47] determined Na, K, and Ca in oyster tissue and low boron glass. Other workers have determined limits of detection of various elements [47-49]. In ref. [49], a He CMP operated at 900 W was used, and the limits of detection that were obtained were comparable to those by Ar-ICP-OES.

Although the CMP is less evaluated with reference to theory and instrumentation than the ICP, available data [19] on performance and applications lead to the following conclusions.

(i) The CMP is stable and insensitive to addition of molecular species. Alkali and alkaline earth metal salts, however, may change the shape of the plasma.

(ii) No ignition problems occur and no tuning (impedance matching) is necessary in most cases.

(iii) N_2-CMPs have spectra that are like those obtained by DC arcs. Common wavelength and line coincidence tables may therefore be used as a first approximation when evaluating an N_2-CMP.

(iv) Most of the CMPs (400 W - 600 W) have shown matrix effects unless ionization buffers are used.

(v) The CMP has potential for the direct analysis of solid, liquid and gas samples.

Instrumentation

The basis of the CMP used in this work is the coupling of microwave energy into and then extracting it from a waveguide. Figure 1-1a shows the configuration of transferring microwave energy into a waveguide and then capacitively coupling the

Figure 1-1. Method of coupling microwaves to and from a rectangular waveguide (i) and a rectangular waveguide showing a and b dimensions (ii).

i

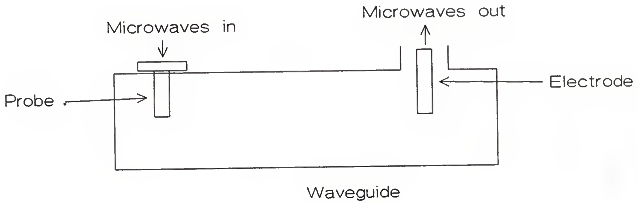
Microwaves in
Microwaves out
Probe
Electrode
Waveguide

ii

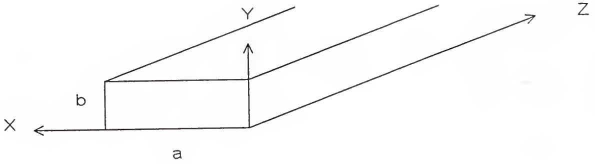
Y
Z
b
X
a

microwaves using an electrode. A CMP is formed if the microwaves which would otherwise radiate from the electrode tip (electrode acting as a microwave antenna) come into contact with a gas. If the power is high enough, auto-ignition of the plasma is achieved. Referring to Figure 1-1a, the components of interest are: the microwave power source, the waveguide, and the electrode system.

Microwave Power Sources

Early microwave plasma systems used medical diathermy units which supplied approximately 125 W to 200 W at 2450 MHz. The increasing popularity of microwave ovens operating at 2450 MHz has reduced the cost and increased the availability of magnetron power sources.

Waveguides

A waveguide consists of a hollow metallic tube of rectangular or cylindrical shape. It is more commonly used at microwave frequencies than coaxial cables because it has higher power handling capabilities. Waveguides are a simpler, lower cost mechanical structure and have lower loss per unit length than coaxial cables since at high power levels coaxial cables tend to radiate and heat up, increasing power loss. In waveguides, the electric and magnetic fields are confined to the space within the walls. No power is therefore lost through radiation [50]. Also dielectric loss is negligible since the waveguides are usually air filled. There is some power loss as heat in the walls due to the skin depth (δ) of the material used in constructing the waveguides, defined as the depth at which the current has decreased to 1/e of the value at the surface (e is the exponential function). The skin depth is smaller for materials of high conductivity, or at higher frequencies because it is inversely proportional to these quantities [51]. Materials with smaller δ values have lower power loss as heat in the waveguides. Some of the δ values for a number of metals at 2450 MHz are Ag, 1.3 μm; Cu, 1.3 μm; Au, 1.6 μm; Al, 1.6 μm; and brass, 2.7 μm [52]. Ag, Cu and Au are difficult to machine and the resulting surfaces may be marred. Also, Ag and Cu surfaces corrode rapidly in air and become less conducting with time while Au is expensive. Because of these reasons, Al and brass are usually used.

Electromagnetic waves in free space may be propagated as: (i) transverse electric magnetic (TEM) waves where the electric and magnetic components are perpendicular to the direction of propagation; (ii) transverse electric (TE), where only the transverse electric wave exists and is perpendicular to the direction of propagation; and (iii) transverse magnetic (TM), where only the transverse magnetic wave exists.

A wave must satisfy the following conditions in order to travel through a waveguide: (i) all electrical flux lines must be perpendicular to the walls of the waveguide, and (ii) all magnetic flux lines at a wall must run parallel to the surface [53]. The TEM mode cannot, therefore, be propagated in a waveguide.

To denote the mode being propagated, two subscripts (m and n) are added to the designation TM and TE. TM_{mn} and TE_{mn} are used, where m and n are integers that define the number of half wavelengths that will fit in the a and b dimensions respectively (see Figure 1-1b). The a-dimension determines the cut-off frequency f_c, the frequency below which no wave propagation occurs. For an air filled waveguide, f_c for the TE_{10} mode is [54]

$$f_c=\frac{c}{2a} \qquad (1)$$

where c is the velocity of light. The actual wavelength in the waveguide, λ_g, is [55]

$$\lambda_g=\frac{\lambda_0}{\sqrt{1-(\frac{f_c}{f})}} \qquad (2)$$

where λ_g is the wavelength in waveguide

λ_o is the wavelength in free space

f_c is the cut-off frequency

f is the operating frequency.

The mode with the lowest cut-off frequency in a particular waveguide is called the dominant mode. The dominant mode in a rectangular waveguide with a<b is the TE_{10} mode, and although it is possible for several modes to exist simultaneously in a given waveguide, only the dominant mode

will propagate, and the higher modes near the source will decay very fast [55].

Coupling Power into and out of Waveguides

The probe, used to introduce microwave energy into the waveguide and the electrode that extracts the microwaves from the waveguide are placed a distance of $\lambda_g/4$ (or an odd multiple of a quarter wavelength) from the ends. Under these conditions, the waves traveling to the edges return in phase with the waves going in the opposite direction since a phase shift of 90° results by travelling the $\lambda_g/4$ distance, a 180° phase shift by the reflection at the wall, and another 90° by travel of the $\lambda_g/4$ distance back to the probe or electrode. Also, at this distance ($\lambda_g/4$) from the edges, there is maximum density of the electric fields, so that there is maximum coupling between the probe and electrode and the microwaves.

Instrumentation Used in this Work

The experimental setup used is shown in Figure 1-2, and the components are listed in Table 1-1. The plasma is generated with a system similar to that reported previously [45], except that a different torch and electrode dimensions, spectrometer, and detector were used. The magnetron is capable of supplying up to 1.6 kW at 2450 MHz. During the course of the work, it was found that the current to the plasma fluctuated randomly. The cause of the fluctuations was not determined, but such fluctuations translated into random fluctuation of emission from the CMP. A current regulator and

Figure 1-2. Experimental set up for CMP system.

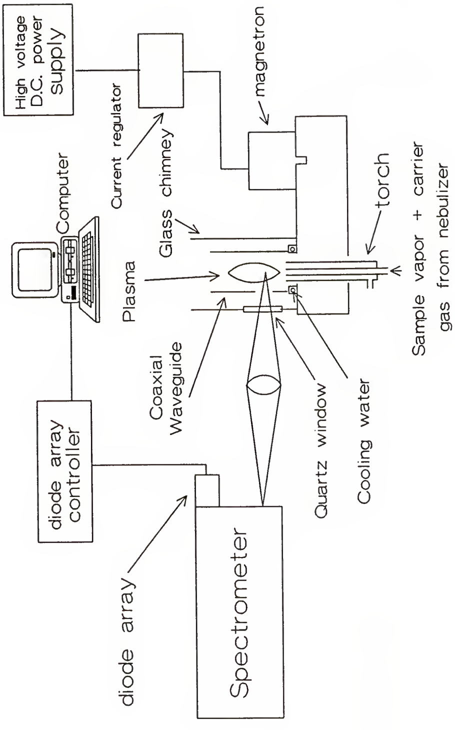
High voltage D.C. power supply
Current regulator
magnetron
Computer
Glass chimney
torch
Sample vapor + carrier gas from nebulizer
Plasma
Coaxial Waveguide
Quartz window
Cooling water
diode array controller
diode array
Spectrometer

Table 1-1. Instruments and components for CMP

Instrument/component	Manufacturer
Diode array: OSMA model IR4-1024	Princeton Instruments, Princeton, NJ, USA
Spectrometer: Jobin-Yvon HR 1000, 1 m, 2400 grooves mm^{-1}, linear dispersion 0.5 nm mm^{-1}	Princeton Instruments
Software (I-120)	Princeton Instruments
OSMA detector controller	Princeton Instruments
PC computer	IBM
High voltage d.c. power supply: 805-1A (maximum power output 1.6kW)	Hipotronics, Brewster, NY, USA
Magnetron: model NL 10251-2 (frequency 2.45 GHz, maximum power output 1.6 kW)	National Laboratories Orlando, Fl., USA
Electrode (SPEX graphite rode; grade HPND)	Laboratory made
Torch: two concentric quartz tubes	Laboratory made

stabilizer circuit (D. Hueber, unpublished results) was used. The current could be held constant at any predetermined level within the working range of the magnetron by operating at a voltage level such that the set current was passing through the circuit. Increasing the voltage further only resulted in an increase in the voltage across the current stabilizing circuit itself and did not lead to any increase in the current passing through the circuit. This resulted in a more stable plasma, improving the precision of the measurements.

For all work involving solution nebulization, the plasma gas used was a mixture of He and H_2 (4.5% H_2), while 2% H_2 was employed for the determination of As, Se and Hg by reduction with $NaBH_4$ (chapter 5).

Helium plasmas have been employed in order to take advantage of the high ionization energy of helium which should result in efficient excitation of the elements introduced into the plasma, especially elements of high excitation energies such as As, halogens, N_2, O_2, Te, and Sn [56]. Limits of detection of chlorine and bromine were lower in a He-ICP-OES compared to Ar-ICP-OES [56].

The electrical resistivity, heat capacity and thermal conductivity for He, however, are greater than for Ar. This leads to faster dissipation of heat towards the torch walls than in the case of Ar, causing difficulty in the design of torch configurations [57] as the He plasma tends to adhere to the torch walls. Work on He plasmas has therefore developed concurrently with special torch designs [57-63]. In Ar CMPs, it is sometimes necessary to wet the plasma gas with water for stability [64,65]. This is not necessary with He CMPs. Like He-ICPs, there is still a tendency, in the system employed for this work, for the plasma to reside at the walls of the torch if pure He plasma gas is used. Addition of a small amount of H_2 (or N_2) solves this problem. The effects of this added hydrogen will be investigated in Chapter 3. Chan and Montaser [56] mention that He ICPs usually require a mixture of other gases such as Ar and air for stability.

The torch used (Figure 1-3) is a two-tube, tangential flow torch made from quartz and has a graphite (solution nebulization) and Ti (hydride generation) electrode inserted in the inner electrode. It has been established by Ali [66] that the optimum length of the electrode portion inside the waveguide should be approximately 3 cm. The rest of the electrode is above the waveguide. Under these conditions, he determined that approximately 100% of the DC power to the magnetron is converted to microwave energy. The microwave power in this work is therefore estimated by taking the product of the current through the magnetron and the voltage across it.

The photodiode array detector used has a 20 nm spectral range. This detection system was particularly advantageous in diagnostic studies (Chapter 2). The detector was characterized by measuring the emission intensity of the mercury 407.8 nm

Figure 1-3. Torch and electrode system (a) and electrode (b). All measurements are in mm.

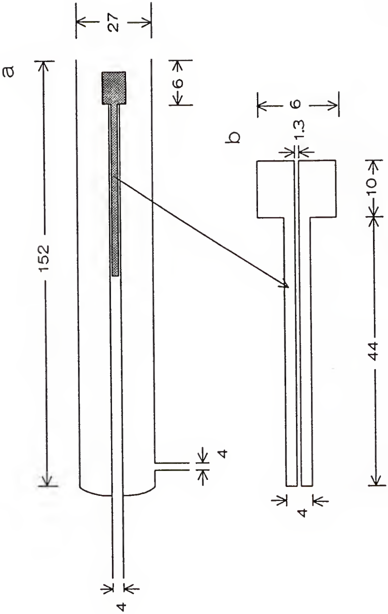
a
27
6
152
4
4
b
6
1.3
10
44
4

line, background and background noise of the radiation from a mercury lamp. During data acquisition, the signal can be integrated for different time intervals, or spectra may be accumulated, or a combination of the two.

Signals were obtained by fixing the integration time for the acquisition of one spectrum to 0.033 s and varying the number of spectra accumulated, and then fixing the number of spectra accumulated to one and then varying the integration time. In each case, the total time taken for integration or accumulation was kept the same. Figure 1-4 shows that similar signal intensities are obtained for the same integration or accumulation times. The intensity is linear with both integration and accumulation times. As expected, longer integration and accumulation times increase the signals obtained. Higher integration and/or averaging times are therefore beneficial for low signals.

Figure 1-5 shows the effect of the integration and accumulation times on the background noise. This was done by using the OSMA software which has the option of calculating the standard deviation of the signal between any diodes directly. The results show that the noise in both cases increases linearly with integration and accumulation time, but the noise due to accumulation is much higher than that due to integration. The signal-to-noise ratios at various integration and accumulation times were plotted and show an initial linear increase which then reaches a plateau (Figure 1-6). Since the

Figure 1-4. Effect of different accumulation and integration times on Hg signal.

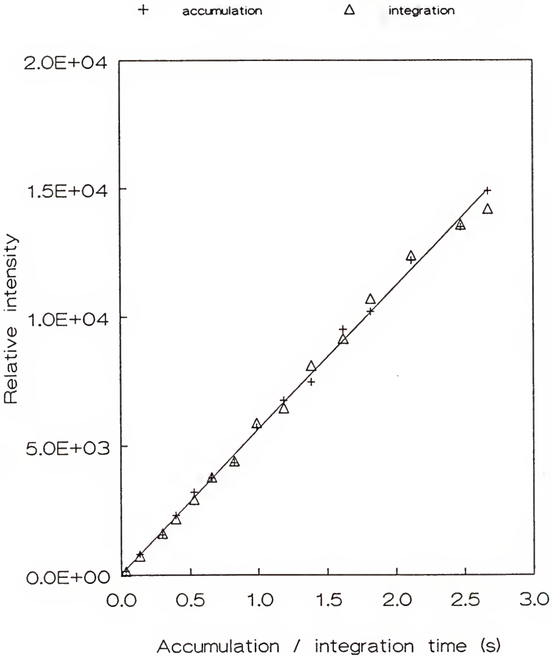
+ accumulation
Δ integration
2.0E+04
1.5E+04
1.0E+04
5.0E+03
0.0E+00
Relative intensity
0.0
0.5
1.0
1.5
2.0
2.5
3.0
Accumulation / integration time (s)

Figure 1-5. Effect of different accumulation and integration times on background noise.

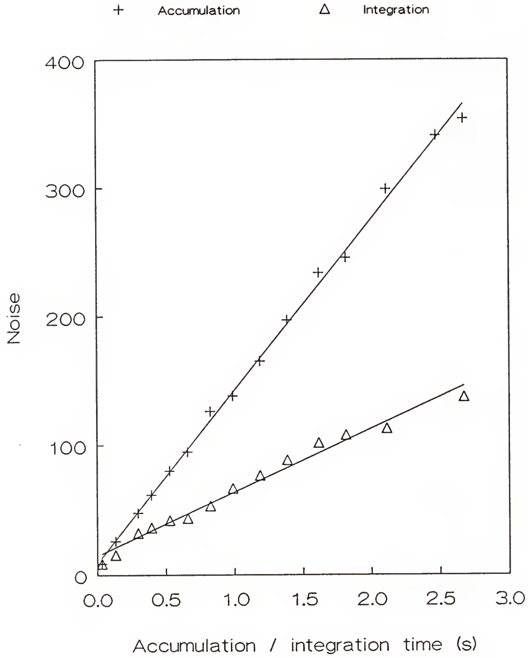
+ Accumulation
Δ Integration
Noise
400
300
200
100
0
0.0
0.5
1.0
1.5
2.0
2.5
3.0
Accumulation / integration time (s)

Figure 1-6. Effect of different accumulation and integration times on signal-to-noise ratio.

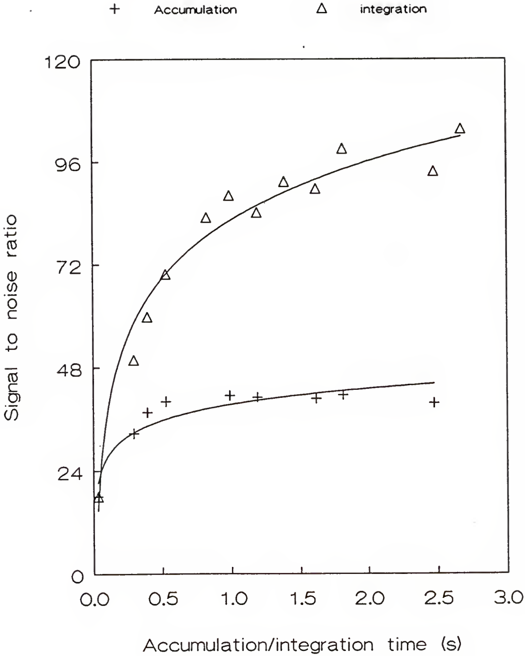
+ Accumulation
△ integration
Signal to noise ratio
0
24
48
72
96
120
0.0
0.5
1.0
1.5
2.0
2.5
3.0
Accumulation/integration time (s)

noise levels of signals that have been accumulated is higher than those for signals that have been integrated, the signal-to-noise ratios for integrated signals are better than those for accumulated signals. Use of integration should result in better signal-to-noise ratios, especially integration and accumulation times above 0.33 s. Also, there is little improvement of signal-to-noise ratios above 1 s and 0.5 s for integration and accumulations respectively.

The Plasma

The plasma formed was almost transparent in nature and therefore its dimensions were difficult to determine. At 700 W, the plasma diameter at its widest part (5 mm above the electrode) was estimated to be 2 cm and the length of the plasma was 7 cm. The plasma became bigger and taller (and more transparent) as the power was increased. The plasma became shorter and fatter as the hydrogen concentration was reduced (see Figure 1-7).

The stability map of the plasma used (95.5% He, 4.5% H_2) is shown in Figure 1-8. The plasma cannot be sustained at power levels less than 100 W for the plasma gas flow rates considered (up to 8 L/min) except for plasma gas flow rates of 6 to 8 L/min where the plasma could be sustained at 50 W. Two hundred watts are required to sustain the plasma for plasma gas flow rates less than 1 L/min. At low flow rates, the plasma tends to form on one side of the electrode and some arcing is observed. Also, at medium flow rates the plasma

Figure 1-7. Dimensions of CMP. (a) 700 W, 4.5% H_2, (b) 800 W, 4.5% H_2 and (c) 700 W, 1% H_2.

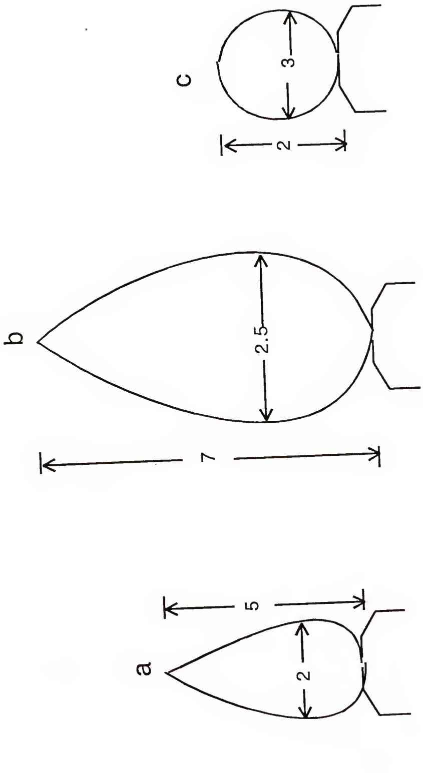
a
5
2
b
7
2.5
c
2
3

Figure 1-8. Stability map of the capacitively coupled microwave plasma.

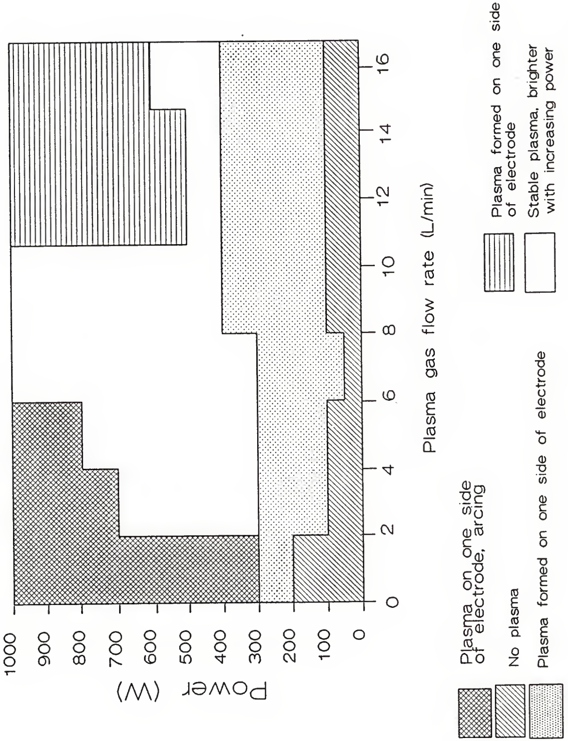
Power (W)
1000
900
800
700
600
500
400
300
200
100
0
0
2
4
6
8
10
12
14
16
Plasma gas flow rate (L/min)
Plasma on one side of electrode, arcing
No plasma
Plasma formed on one side of electrode
Plasma formed on one side of electrode
Stable plasma, brighter with increasing power

tends to form on one side as well, but no arcing is observed in this case. At very high flow rates and power levels, the plasma forms on one side of the electrode. The best conditions to operate the plasma are flow rates of 6-8 L/min where the plasma is stable over a wide power range.

CHAPTER 2
DIAGNOSTIC STUDIES

Introduction

A plasma is defined as a gas or vapor in a partially ionized state, and thus is composed of atoms, molecules, ions and free electrons [67]. One of the problems in plasma chemistry or physics is the determination of the plasma state, i.e. quantitative determination of the chemical constitution of the plasma including the number of free electrons present, and determination of such parameters as temperature, specific heat, viscosity, and thermal and electrical conductivity [68].

Spectroscopic methods are preferred to other methods in plasma diagnostic studies because they have no disturbing effect on the plasma during measurements, as is the case with probe measurements, and information content of the signals obtained may be very large. If the spectral intensity of one line and its vicinity is measured, the wavelength gives information that a certain element is present in a certain stage of ionization. The line profile contains information on the kinetic temperature of the emitting atom (Doppler broadening) or the density of perturbing particles (pressure broadening). The total energy emitted in the line allows conclusions regarding the excitation temperature and the particle density of the emitting species.

In this chapter, the He-H_2 plasma is characterized by the determination of electronic excitation temperature (T_{el}), rotational temperature (T_{rot}), and electron number density (n_e). The effect of power, observation position, solution uptake rate, and carrier gas flow rate on these parameters was evaluated.

Theory

Electronic Excitation Temperature

Treatments for expressions for electronic excitation temperature may be obtained from [68, 69]. The measured intensity of a spectral line is given by

$$I = Ah\nu n_k\theta \qquad (1)$$

where I is the integrated intensity, A is the Einstein transition probability for spontaneous emission, h is Planck's constant, ν is the frequency of the emitted radiation, n_k is the number of probe atoms in level k, and θ is an instrumental factor.

The Boltzmann distribution allows us to define the ratio of populations or number densities n_j and n_k of the probe atoms in the states of energy E_j and E_k with k > j.

$$n_k/n_j = (g_k/g_j)\ \exp[-(E_k - E_j)/kT_{el}] \qquad (2)$$

where g_k and g_j are the statistical weights of the two levels (g = 2J+1). If we consider the total number density of the ionization state in question, we have,

$$n_k/n = [g_k \exp(-E_k/kT_{el}]/Q(T) \quad (3)$$

where T_{el} is the electronic excitation temperature, n is the number density of the probe atoms summed over all energy levels, and Q(T) the internal partition function defined as:

$$Q(T) = \sum_k g_k \exp[-E_k/kT_{el}] \quad (4)$$

For the case where the ground state is the only state appreciably populated, Q(T) is approximately equal to g_0, where g_0 is the statistical weight of the ground state. Using equation (3) and (1),

$$I = h\nu_k \theta A_k n g_k \exp[-E_k/kT_{el}] \quad (5)$$

By measuring more than one spectral line, a knowledge of absolute intensities required by equation (5) can be replaced by more easily measured relative intensities

$$\frac{I_k}{I_j} = \frac{A_k h\nu_k \theta n g_k Z^{-1} \exp(-E_k/kT_{el})}{A_j h\nu_j \theta n g_j Z^{-1} \exp(-E_j/kT_{el})} \quad (6)$$

$$\frac{I_k}{I_j} = \frac{A_k g_k \nu_k}{A_j g_j \nu_j} \exp[-(E_k-E_j)/kT_{el}] \quad (7)$$

All the factors in equation 5 can either be measured or obtained from tables, hence the temperature can be determined. To reduce uncertainties, equation (5) may be rearranged to the following form,

$$I = h\nu_k \theta A_k n g_k e^{-E_k/kT_{el}} = \frac{hc}{\lambda}\theta A_k n g_k \exp(-E_k/kT_{el})$$

$$\frac{I\lambda}{A_k g} = (hc\theta n)\exp(-E_k/kT_{el})$$

$$\log\frac{I\lambda}{gA} = \log(hc\theta n) - \frac{E_k}{2.303kT} \qquad (8)$$

Also if λ is expressed in nm and since

$$g_k A = \frac{Cg_i f}{\lambda^2} \qquad (9)$$

where $C = 6.67 \times 10^{13}$ $nm^2 s$, then

$$\log\frac{I\lambda^3}{Cgf} = \log(hc\theta n) - \frac{E}{2.303kT} \qquad (10)$$

$$\log\frac{I\lambda^3}{gf} = \log C + \log(hc\theta n) - \frac{E}{2.303kT_{el}}$$

A plot of $\log(I\lambda/gA)$ or $\log(I\lambda^3/gf)$ versus E_i, the energy of the upper level for several lines, should yield a straight line, whose slope is $-0.43/kT$. Thus the electronic excitation temperature temperatures may be determined.

Rotational Temperature from Band Systems of Diatomic Molecules

The rotational intensity distribution in the fine structure of a band of a diatomic molecule may be utilized in the determination of rotational temperatures. For a rotational transition, the intensity of emission due to a transition from state J to J' is given [70] by:

$$I = C_1 n_J A_{JJ'} h\nu_{JJ'} \tag{14}$$

where C_1 is a constant including parameters from the measuring apparatus, n_J is the number of molecules in state J, $A_{JJ'}$ is the transition probability, and $\nu_{JJ'}$ is the frequency of the transition. The number of molecules in state J is given by:

$$n_J = \frac{n_t}{Q_R}(2J+1)\ \exp(-E_r/kT_{rot}) \tag{12}$$

where n_t is the total number of molecules, Q_r is the rotational partition function, and E_r is the rotational energy, given by $-B_rJ(J+1)hc$ where B_r is the rotational constant, in cm^{-1}, for the upper state. Combining (11) and (12) yields,

$$I = C_1 A_{JJ'} h\nu\,(\frac{n}{Q_R})\ (2J+1)\ \exp(-E_r/kT)\,. \tag{16}$$

Letting $C_2 = C_1 h$, then

$$I = C_2 A_{JJ'} \nu\,(\frac{n}{Q_R})\,(2J+1)\exp(-\frac{E_r}{kT})\,. \tag{14}$$

Taking logarithms of both sides gives

$$\log I = \log(\frac{C_2 n_t}{Q_R}) + \log(A_{JJ'}\nu\,(2J+1)) - \frac{E_r}{2.303kT}\,. \tag{18}$$

Letting $\nu = c/\lambda$, $A_{JJ'}$ $(2J+1) = A$, and $C_3 = \log(C_2 n_t/Q_R)$,

$$\log\frac{I\lambda}{A} = C_3 - \frac{E_r}{2.303kT} \tag{19}$$

The values for log $(I\lambda/A)$ are plotted versus the energies of the upper rotational state, E_R, and the slope of the resulting line is $-1/2.303kT$.

Electron Number Densities

Spectral lines from plasmas are broadened by interaction between the emitting atoms and the local electric field generated by the surrounding ions and electrons. This phenomenon is called Stark broadening. Atomic hydrogen is subject to an exceptionally large Stark effect so that Stark broadening is dominant over Doppler broadening, in most cases.

The method used to determine electron number densities in this work is based upon the Stark broadening of the H_β (486.1 nm) line. The line profile of the line is described [70] by a distribution function $S(\alpha)$ which is normalized such that

$$\int_{-\infty}^{\infty} S(\alpha)\, d\alpha = 1$$

The value of α is given by $\alpha = \Delta\lambda/F_0$ where $\Delta\lambda$ is some measurement of the width of the peak (Å) and F_0 is the field strength given by $F_0 = 1.25\times10^9 n_e^{2/3}$. When the full width at half maximum is used, the above expressions give [70,71],

$$\Delta\lambda_s = 2.50\times10^{-9}\alpha_{1/2} n_e^{2/3} \tag{17}$$

where $\alpha_{1/2}$ is the semi-half-width of the reduced Stark profile, obtainable from tables.

Experimental

The instrument described in chapter 1 (using graphite electrodes) was employed in the determination of T_{el}, T_{rot} and n_e values. The use of a photodiode array detector for temperature measurements has several advantages over scanning methods [72]: the spectra can be acquired rapidly, and since the intensities of all lines are measured simultaneously, errors in the relative intensities measured are minimized. Spectral background resulting from solvent species and electrode or plasma background can be conveniently removed if necessary. Lines and instrument conditions were chosen such that: (1) the lines of interest fell within one wavelength window; (2) there was no significant overlap of the lines, and (3) the line intensities fell within the dynamic range of the array during a fixed integration time. All the diagnostics were carried out at 700 W unless specified otherwise. For radial and axial measurements, a spectrometer entrance slit width and slit height of 0.02 mm and 2 mm, respectively, were used while for all other measurements, slit height of 4 mm and slit width of 0.04 mm were used. Unless stated otherwise, 700 W and an observation height of 5 mm above the electrode were used in all cases. The plasma gas and carrier gas flow rates were kept constant at 6 L/min and 900 mL/min respectively.

Measurement of Electronic Excitation Temperature

Iron excitation temperatures were measured using six emission lines in the 370-377 nm region. Intensities of the following lines (nm) were used for the Boltzmann plot: 372.0, 373.7, 374.8, 374.9, 375.8 and 376.4. Iron was used because it has well known transition probabilities and oscillator strengths, wide energy range, and closely spaced wavelengths so that calibration of the detector for spectral response was not necessary. In order to increase the resolution, the second order setting on the spectrometer was used. Figure 2-1 shows a typical iron spectrum obtained in this work. Average gf values from references [73-76] were used (see Table 2-1). The iron spectra were obtained by aspirating iron solutions (10 ppm - 100 ppm) into the plasma.

Measurement of Rotational Temperature

Rotational temperatures were determined from relative intensities of rotational lines of the Q_1 branch of the (0,0) transition of the OH radical in the 307 nm - 310 nm region. In order to resolve the lines, the fourth order setting of the spectrometer was used. Figure 2-2 shows the spectrum obtained in this region. The spectra were obtained while aspirating water into the plasma. The A values used for the Boltzmann plot were taken from ref. [77] (see Table 2-2). Five lines ($Q_1 2$, $Q_1 4$-$Q_1 6$, $Q_1 9$) were used. The temperature was obtained

Figure 2-1. A typical spectrum of the neutral iron emitted by the CMP.

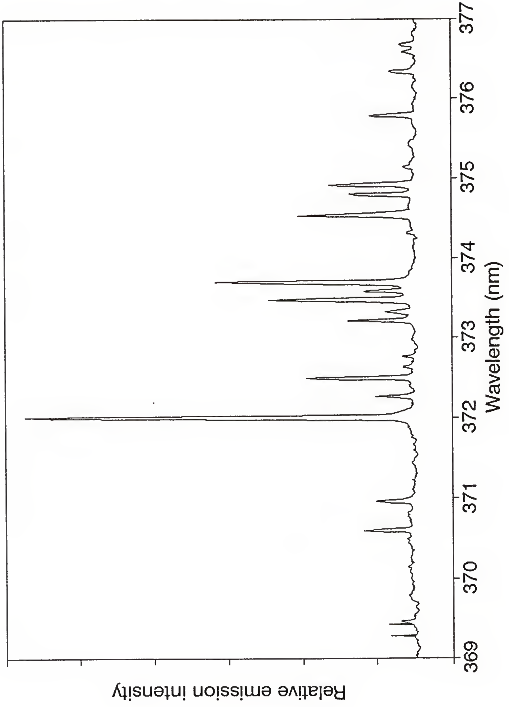
Relative emission intensity
Wavelength (nm)
369
370
371
372
373
374
375
376
377

Table 2-1. Wavelengths, excitation energies and log gf values for neutral iron used for excitation temperature measurements.

λ (nm)	E (cm^{-1})	Ref. 73	Ref. 73	Ref. 75	Ref. 76	Average
373.7	27167	-0.57	-0.57	-0.57	-0.58	-0.575
374.8	27560	-0.98	-1.01	-1.00	-	-0.997
374.9	34040	0.18	0.17	-	0.16	0.170
375.8	34329	0.00	0.00	-	-0.03	-0.010
376.4	34547	-0.18	-0.19	-	-0.24	-0.203

Table 2-2. Assignment, wavelengths, energies, and A values for the Q_1 branch of the OH (0-0) band used for rotational temperature measurements.

K	λ (nm)	E (cm^{-1})	A (10^8 s^{-1})
2	307.995	32543	17.0
4	308.324	32779	33.7
5	308.520	32948	42.2
6	308.734	33150	50.6
9	309.534	33952	75.8

Figure 2-2. A typical spectrum of the (0,0) band of OH emitted by the CMP.

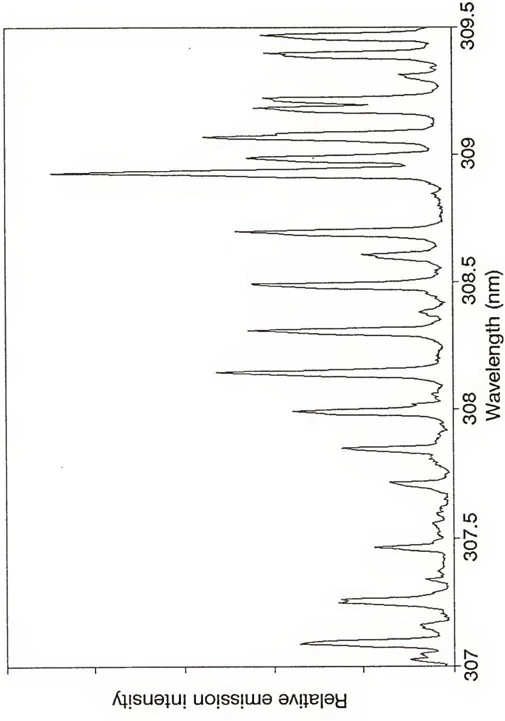
Relative emission intensity
Wavelength (nm)
307
307.5
308
308.5
309
309.5

from the slope of the log(Iλ/A) versus E (in cm^{-1}) plot. In all cases, straight lines were obtained.

Electron number density determinations

For the determination of the electron number density, the spectrometer was set to its second order setting to record the H_β line. The FWHM was then measured, from which the electron number density could be calculated using the equation $\Delta\lambda_s=2.50x10^{-9}\alpha_{1/2}n_e^{2/3}$ where $\alpha_{1/2}$ is the semi-half width of the reduced profile; $\alpha_{1/2}$ values of 5000 K [71] were used.

Results and Discussion

Effect of Radial Position

Figures 2-3 and 2-4 show the effect of the radial position on T_{el}, T_{rot} and n_e. In all three cases, the temperatures and electron number densities are almost constant across the plasma within the distances measured. T_{el} had a slight dip -1 mm from the center of the plasma but the difference between the highest and lowest temperatures determined was only 200 K. T_{rot} showed the same trend except that the slight dip was at +1 mm from the plasma center. There is also a decrease of T_{rot} at -4 mm from the plasma center. Again the variations are rather small with a temperature range of about 400K. The electron density showed a very slight increase in the electron density near the center of the plasma but the difference between the n_e values in the range was still very small.

Figure 2-3. Electronic excitation temperature (a) and rotational temperature (b) vs radial distance. The plasma was operated at 700 W and viewed 5 mm above the electrode.

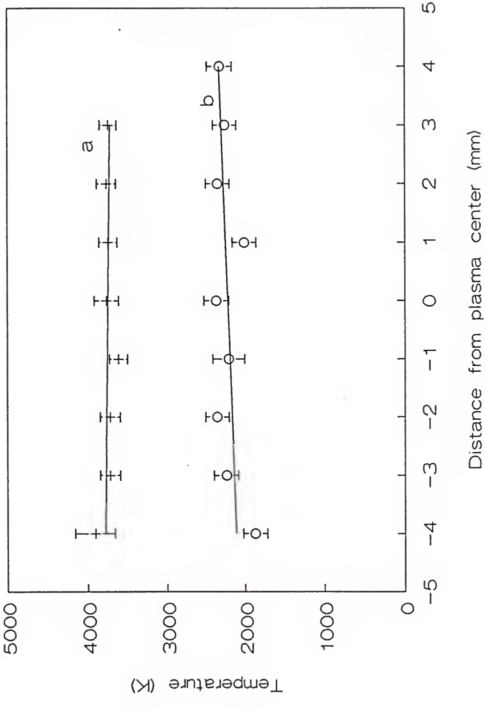
Temperature (K)
0
1000
2000
3000
4000
5000
Distance from plasma center (mm)
−5
−4
−3
−2
−1
0
1
2
3
4
5
a
b

Figure 2-4. Electron number density vs radial distance. The plasma was operated at 700 W and viewed 5 mm above the electrode.

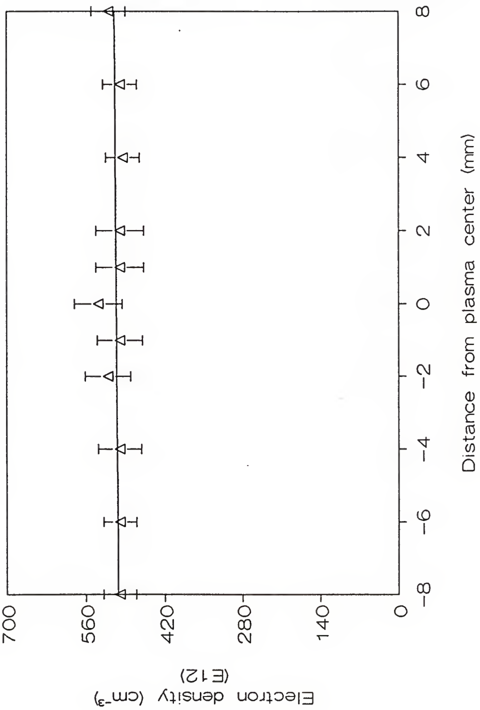
Electron density (cm^{-3})
(E 12)
700
560
420
280
140
0
−8
−6
−4
−2
0
2
4
6
8
Distance from plasma center (mm)

The T_{el} results are in qualitative agreement with other workers. Workman et al. [78] observed a minimum T_{el} at the center of their He MIP. Their electronic excitation temperatures, however, were higher (about 6000 K) than those observed in this work. The range of their temperature values was still small (about 800 K). Tanabe et al. [79] also observed a minimum T_{el} at the center of their He MIP, but the temperature increased rapidly on one side of the plasma, probably indicating an off-center plasma with substantial wall contact [78].

Tanabe et al. [79] observed constant T_{rot} across the plasma, while Workman et al. [78] observed either a minimum or a maximum temperature at the center of the plasma. Heltai et al [80] observed a minimum T_{rot} at the center of the plasma and a maximum at the edges. T_{rot} (using N_2^+) in a He MIP showed the same trend [81].

Brown et al. [82] observed maximum n_e off center at 360 W but the electron number density was spatially independent of position at low power. Tanabe et al. [79] observed a maximum n_e near the center of the plasma.

Effect of Axial Position

The T_{el}, T_{rot}, and n_e generally decreased with increase in distance from the electrode (Figures 2-5 and 2-6). T_{rot}, however, increased from 2400 K to 2800 K (at 4 mm above the tip of the electrode), then decreased slowly as the distance

Figure 2-5. Electronic excitation temperature (a) and rotational temperature (b) vs axial distance. The plasma was operated at 700 W.

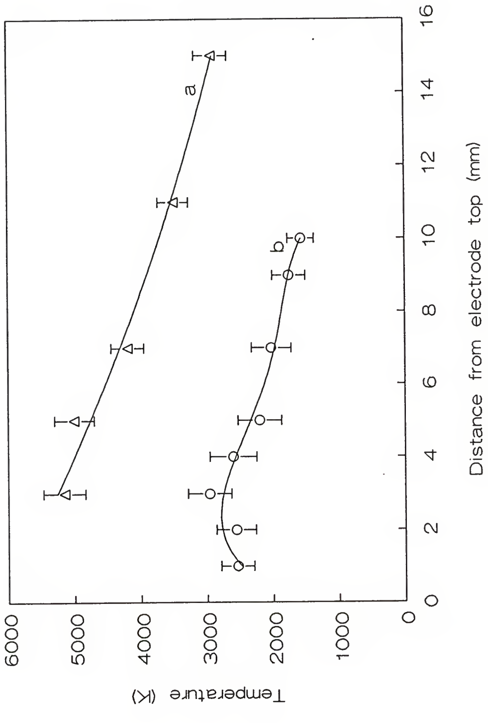
Temperature (K)
6000
5000
4000
3000
2000
1000
0
0
2
4
6
8
10
12
14
16
Distance from electrode top (mm)
a
b

Figure 2-6. Electron number density vs axial distance. The plasma was operated at 700 W.

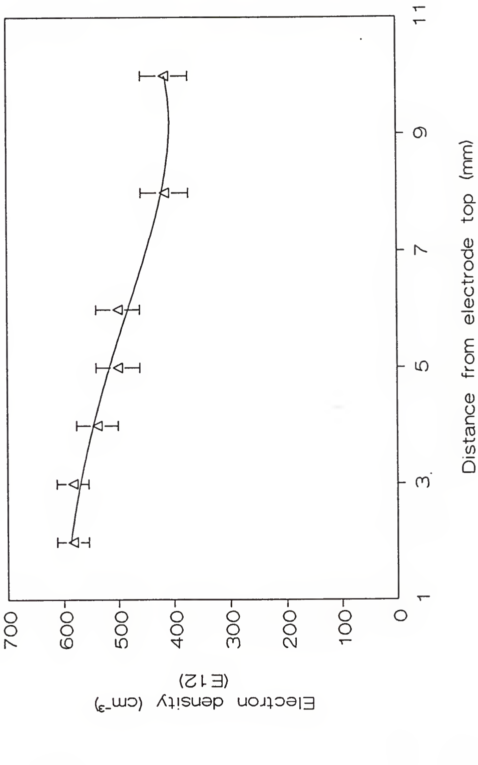
Electron density (cm^{-3})
(E 12)
0
100
200
300
400
500
600
700
1
3
5
7
9
11
Distance from electrode top (mm)

was increased. Electron density measurements made 2 and 3 mm above the electrode were the same and then decreased with increased observation height. The excitation temperature showed the steepest decrease with observation distance. The plasma gets cooler as the observation distance is increased and this is reflected in the decrease of both the electronic excitation temperature and the rotational temperature. Less ionization is also expected in the cooler environment, resulting in low n_e values. We are not able to explain the initial increase in the rotational temperature. Although high T_{el}, T_{rot}, and n_e values were obtained very close to the electrode tip, all other observations were carried out at 5 mm above the electrode tip in order to avoid the high background due to the electrode.

Effect of Carrier Gas

There was a slight increase of T_{el} as the carrier gas flow rate was increased (Figure 2-7a). Since water was being aspirated into the plasma, this increase in excitation temperature may be a result of an increase in the amount of water entering the plasma together with the carrier gas. Increase in T_{el} as the amount of water entering plasma is increased has also been observed in Ar plasmas [83, 84].

T_{rot} was found to be independent of carrier gas flow rate (Figure 2-7b). The same behavior was observed for n_e values where n_e was found to be independent of carrier gas flow rate (Figure 2-8).

Figure 2-7. Electronic excitation temperature (a) and rotational temperature (b) vs carrier gas flow rate. The plasma was operated at 700 W and viewed 5 mm above the electrode.

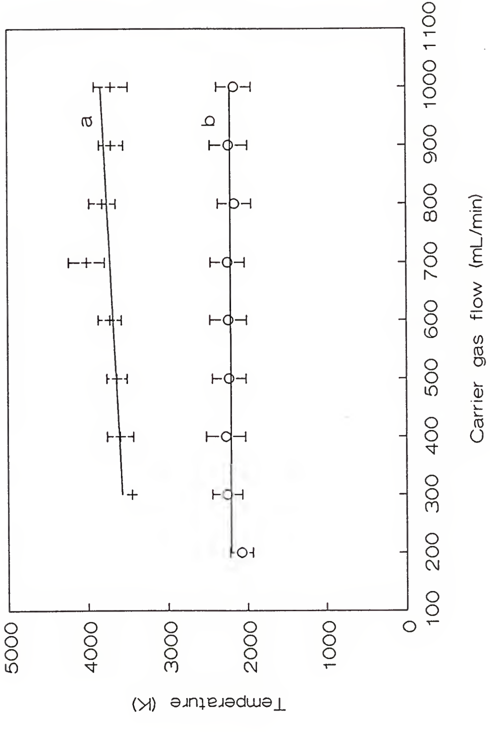
Temperature (K)
5000
4000
3000
2000
1000
0
Carrier gas flow (mL/min)
100
200
300
400
500
600
700
800
900
1000
1100
a
b

Figure 2-8. Electron nuber density carrier gas flow rate. The plasma was operated at 700 W and viewed 5 mm above the electrode.

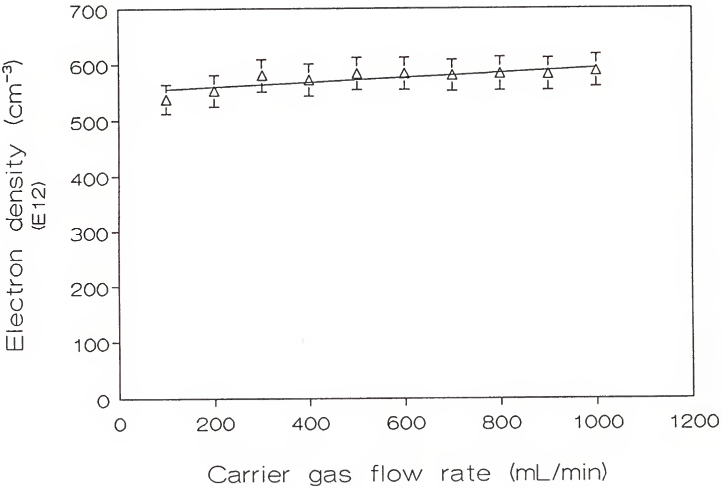
700
600
500
400
300
200
100
0
Electron density (cm^{-3})
(E12)
0
200
400
600
800
1000
1200
Carrier gas flow rate (mL/min)

Effect of Solution Uptake Rate

T_{el} and T_{rot} (Figure 2-9) were found to be almost independent of solution flow rate to the nebulizer (solution pump flow rate), but the electron number density increased slightly until solution uptake rate of 0.8 mL/min then decreased (Figure 2-10). The initial increase in n_e is in agreement with Heltai et al. [80] and may be due to an increase in the amount of water introduced into the plasma.

Effect of Power

Both T_{rot} and T_{el} increased as the power was increased, reaching a plateau at about 600 W (Figure 2-11). This is expected since more energy is provided to the plasma. These results are in agreement with those obtained by other workers [78,79,81] but differ from those obtained by Goode et al. [85] where the T_{el} and T_{rot} were independent of power, probably because they were operating in the plateau region of the temperature/power plot for their plasma. The n_e results showed a different behavior from those exhibited by the temperature curves. The electron number densities were constant with applied power until 700 W and then increased slightly (Figure 2-12). In this work, the n_e values are always higher with water aspiration. Constant electron number densities were observed in the 350-450 W range for an Ar plasma 2 mm off the central axis by Brown et al. [86], but an increase with power was observed when observations were carried out at the plasma

Figure 2-9. Electronic excitation temperature (a) and rotational temperature (b) vs solution uptake rate. The plasma was operated at 700 W and viewed 5 mm above the electrode.

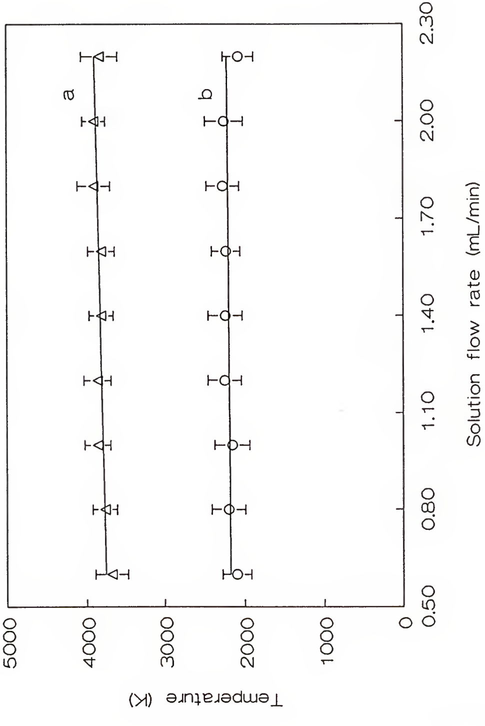
Temperature (K)
5000
4000
3000
2000
1000
0
0.50
0.80
1.10
1.40
1.70
2.00
2.30
Solution flow rate (mL/min)
a
b

Figure 2-10. Electron number density vs solution uptake rate. The plasma was operated at 700 W and viewed 5 mm above the electrode.

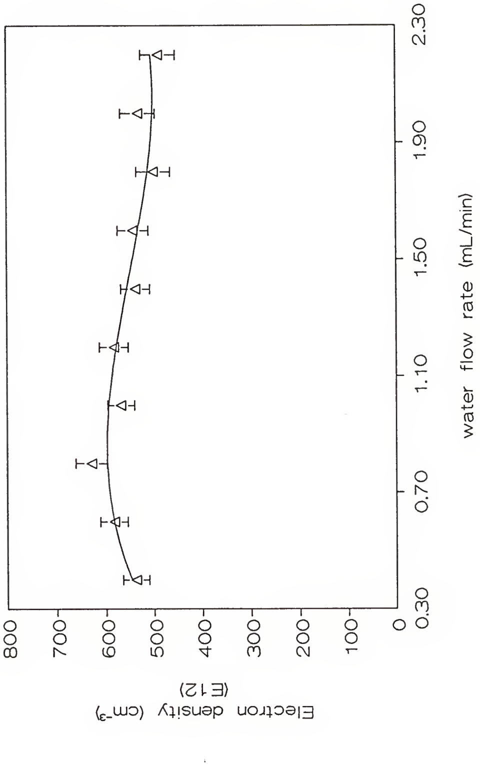
Electron density (cm^{-3})
(E 12)
0
100
200
300
400
500
600
700
800
0.30
0.70
1.10
1.50
1.90
2.30
water flow rate (mL/min)

Figure 2-11. Electronic excitation temperature (a) and rotational temperature (b) vs power. The plasma was operated at 700 W and viewed 5 mm above the electrode.

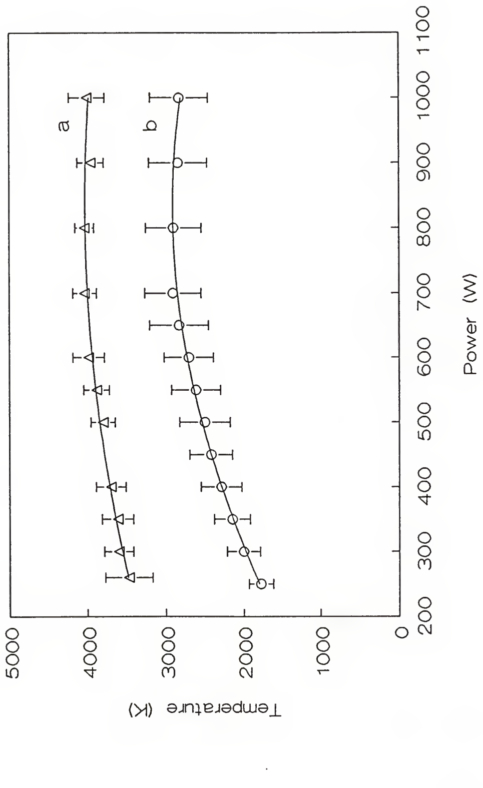
Temperature (K)
5000
4000
3000
2000
1000
0
Power (W)
200
300
400
500
600
700
800
900
1000
1100
a
b

Figure 2-12. Electron number density with and without water aspiration into the plasma vs power. The plasma was operated at 700 W and viewed 5 mm above the electrode.

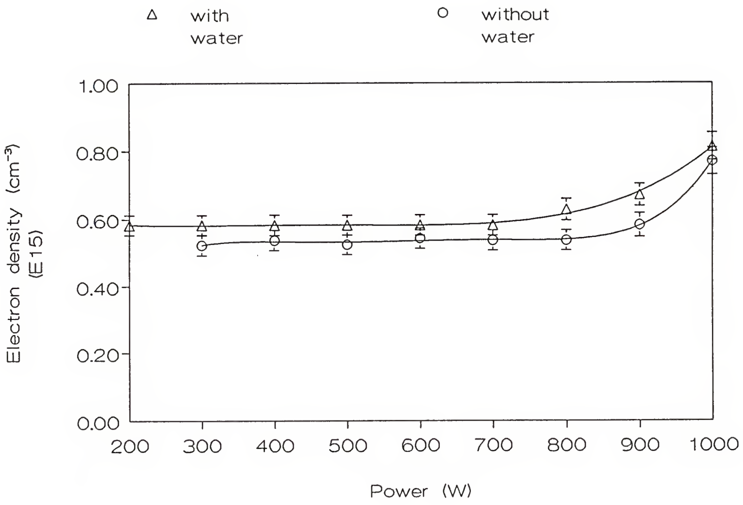

△ with water
○ without water
1.00
0.80
0.60
0.40
0.20
0.00
Electron density (cm^{-3})
(E15)
200
300
400
500
600
700
800
900
1000
Power (W)

center. They observed an initial increase in n_e up to 300 W and then a decline to 400 W in a He plasma.

Summary

In this work, the electronic excitation temperature, rotational temperature, and electron densities were determined and found to be of similar magnitude as those determined by other workers for helium microwave plasmas. The electronic excitation temperature obtained by other workers has been in the range 3000 K to 4500 K [79,87], which compares well with our T_{el} of about 4000 K. Workman et al. [78] and Ali [66] obtained T_{el} of about 6000 K. T_{rot} values reported for He plasmas generally fall in the range 1300 K to 2500 K [87,88,66, 79, 81]. T_{rot} values determined in this work varied between 1800 K and 3000 K. Workman et al. [78] obtained dual-slope Boltzmann plots for T_{rot} determination. Using the "lower slope region" T_{rot} values as high as 8500 K were obtained, indicating the sensitivity of the rotational temperature on plasma gas flow rate. The electron number densities determined in this work ($4x10^{14}$ cm^{-3} - $9x10^{14}$ cm^{-3}) compare well with those obtained by Brown et al. [86] ($5x10^{14}$ cm^{-3} -$2.6x10^{15}$ cm^{-3}) and differ by a factor of approximately 10 compared to those obtained by Tanabe et al. [79] ($3x10^{13}$ cm^{-3} - $1.4x10^{14}$ cm^{-3}). It is remarkable that the different helium plasmas evaluated under various operational conditions have such uniformity in temperatures and electron number densities. Similar results have been obtained by other workers, e.g. [66,78,79].

An interesting feature of the He microwave plasma is the independence of T_{el}, $T_{rot,}$ and n_e for virtually all experimental variables. The only parameter which affected these measurements in this work were power and axial observation distance. The difference in T_{rot} and T_{exc} indicate non-local thermodynamic equilibrium (LTE) conditions in the He CMP.

CHAPTER 3
EFFECT OF HYDROGEN ON PLASMA CHARACTERISTICS

Introduction

Helium plasmas are difficult to form as they tend to reside on the walls of the plasma, reducing the lifetime of the torch and introducing torch material into the plasma. Addition of a small amount of hydrogen was found to eliminate this problem. The plasma so formed was centered in the torch, with the plasma becoming thinner (and taller) as the proportion of the hydrogen was increased. The reduction of plasma size with the addition of molecular species has been observed in ICPs [89-92] and has been attributed to the smaller electrical diameter of these plasmas compared to Ar plasmas [89], to absorption of energy upon dissociation of the molecular species [90] leading to a cooler surface of the plasma, and to less conductivity resulting in thermal pinch. This chapter discusses the effect the added hydrogen has on T_{el}, T_{rot}, n_e and emission signals of Zn, Cr, As, and Hg.

Mixed gas plasmas are not used as much as the pure Ar-ICPs but there are cases where their use is found to be beneficial. Since its introduction in 1965 [93,94] as a gas chromatographic detector, the MIP has been used as an atomization and excitation source for atomic emission spectrometry. Recently a GC detector using MIP emission with a movable photodiode array detector [95] has been introduced. Work on GC detection using microwave excitation usually results in material deposition on the discharge tube walls, the problem being worse for inorganic compounds prone to formation of refractory species [96]. In such cases other gases are added to the plasma gas in order to prevent the formation of these deposits. Carbon deposits are by far the most common nuisance [95-97] and may be prevented by the use of oxygen at concentrations less than 2.5% v/v [95]. Nitrogen may also be used for prevention of C [96,97] and P [98] deposits.

In the determination of elements from inorganic compounds (after conversion to a volatile form and GC separation) Serravallo and Risby [99] were unable to observe a Cr signal unless O_2 was added as a dopant gas to the He plasma gas. The increase in Cr signal however reached a maximum and quickly decreased as the partial pressure of oxygen was increased. The added oxygen also reduced molecular bands arising from species such as N_2, N_2^+, CH, and CN. Estes et al. [100] found that if the plasma was continuously doped with hydrogen, the emission signals for B, Al, Ge, Sn, Pb, P, and As improved 2 - 3 times. The response for transition metals and other main group metals were adversely affected by the introduction of hydrogen, attributed to quenching of the He excitation mechanism [101].

Compared to Ar-ICPs, mixed-gas and molecular gas ICPs offer the advantage of greater heat transfer to analyte aerosol particles. Under certain conditions, the detection limits obtained with these non-Ar discharges are superior to those achieved with the Ar-ICP. High power, mixed gas, and molecular gas discharges have an axial channel that appears to be closer to local thermal equilibrium.

Based on the discussion above, it would be expected that the H_2/He plasma used in this work would have different properties compared to a pure He plasma.

Experimental

T_{el}, T_{rot}, and n_e were determined at 700 W at different concentrations of hydrogen in the plasma gas. The He plasma gas flow rate was kept constant at 6 L/min and the hydrogen flow rate (which was subsequently mixed with the He) was varied so that its concentration varied to about 14 % (v/v). The volume of added hydrogen was assumed to be negligible compared to the He plasma gas. An observation height of 5 mm was used in all cases. The diagnostic parameters were determined using the same methods as in chapter 2: Fe was used for the determination of T_{el}, OH, for T_{rot} and the H_β line for n_e. Since the plasma gas already contained hydrogen, no additional hydrogen was added in the determination of n_e. Emission signals, and signal-to-noise ratios (S/N) were determined at 800 W for Zn (10 ppm, at 481.05 nm) and Cr (5 ppm at 425.43 nm) using direct sample nebulization, and As and

Hg, by direct introduction of AsH_3 gas and Hg vapor into the plasma. For AsH_3, 50 ppm AsH_3 in He from a cylinder (supplied by Alpha Gas, Jacksonville, Fl. USA) was diluted with He and introduced into the plasma. The emission signal from the As was measured using the 228.8 nm line. For Hg, He was swept above a pool of Hg in a closed container. The He/Hg mixture was then mixed with additional He and introduced directly into the CMP. The 435.8 nm line was used for Hg detection.

Results and Discussion

Electronic Excitation Temperature

T_{el} decreased gradually as the hydrogen concentration was increased (Figure 3-1a). This reduction is a result of H_2 quenching microwave energy and reducing the overall excitation energy of the plasma [96]. Since molecular species can absorb microwave energy thereby exciting vibrational modes, the absorbed energy is not available for excitation.

Abdallah and Mermet [87] found no difference in T_{el} for pure Ar and Ar- N_2 (7.5%) MIPs. Blades and Caughlin [72] observed lower T_{el} when xylene was aspirated into an Ar plasma compared to temperatures obtained when aqueous solutions were introduced into the plasma for the same power level. Power levels of 0.55 kW higher than those used for aqueous solutions were required in order to obtain similar T_{el}.

Rotational Temperature

T_{rot} increased with increase in hydrogen concentration

Figure 3-1. Effect of hydrogen on electronic excitation temperature (a) and rotational temperature (b) at 700 W.

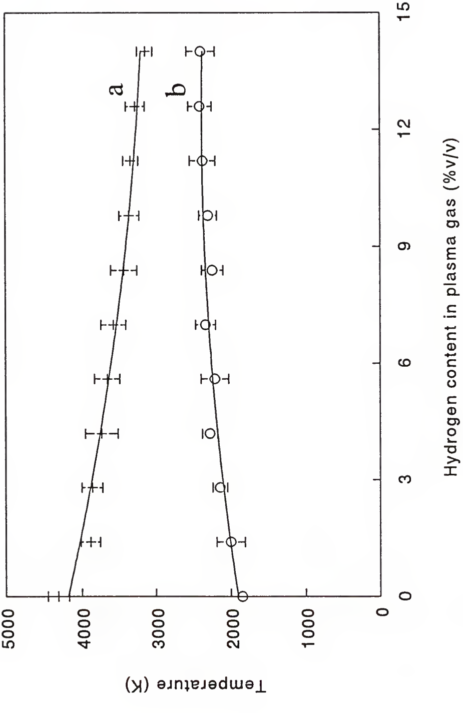
Temperature (K)
5000
4000
3000
2000
1000
0
Hydrogen content in plasma gas (%v/v)
0
3
6
9
12
15
a
b

(Figure 3-1b). T_{rot} is usually taken to reflect the actual plasma temperature. These results are therefore in agreement with those by Cobine and Wilbur [23] where a slight addition of molecular species to inert gases resulted in higher temperatures capable of melting tungsten when it was not even possible to ignite a piece of paper using the pure inert gas. The increase in the rotational temperature may be a result of the heat of association of atoms dissociated by the microwaves. Abdalla and Mermet [57] observed a slight increase of T_{rot} in a Ar-N_2 10%) plasma (T_{rot} 2900) compared to a pure Ar plasma (T_{rot} 2570). A less pronounced effect was observed using a He (T_{rot} 2030) and a He-N_2 (7.5%) plasma (T_{rot} 2050). In either case, a slight temperature increase was observed.

Electron Number Density

The electron number density increased as the hydrogen concentration was increased from 2 % to 10 % and then declined (Figure 3-2). The increase at low hydrogen concentrations is probably due to ionization of the added hydrogen (similar to the ionization of water described in Chapter 2). This increase is offset at higher hydrogen concentrations because the energy available is not sufficient to dissociate and ionize the increasing amount of hydrogen. The same trend was observed for different amounts of water in the plasma (Figures 2-10).

Effect on Emission Signals

Figures 3-3 to 3-6 show the signal, and signal-to-noise ratios versus concentration of hydrogen for Zn, Cr, As, and

Figure 3-2. Effect of hydrogen on electron number density. The plasma was operated at 700 W.

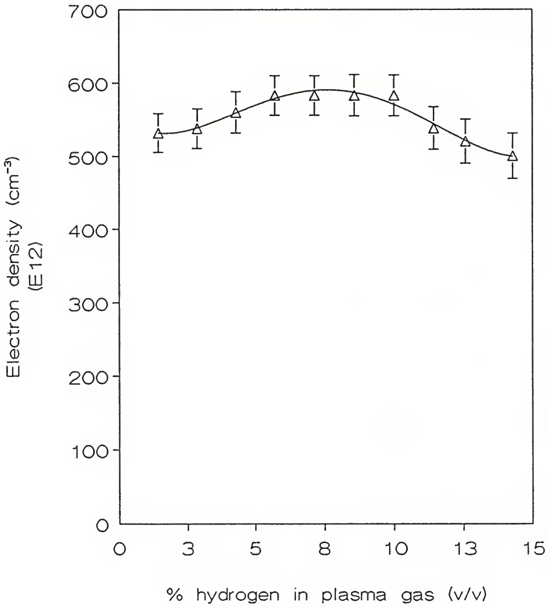
700
600
500
400
300
200
100
0
0
3
5
8
10
13
15
Electron density (cm^{-3}) (E12)
% hydrogen in plasma gas (v/v)

Figure 3-3. Effect of hydrogen on Zn emission signal and signal-to-noise ratio. The plasma was operated at 800 W.

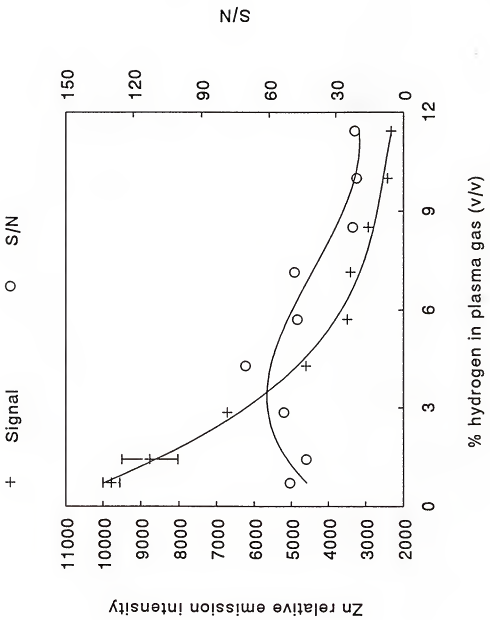
+ Signal
○ S/N
Zn relative emission intensity
11000
10000
9000
8000
7000
6000
5000
4000
3000
2000
% hydrogen in plasma gas (v/v)
0
3
6
9
12
S/N
150
120
90
60
30
0

Figure 3-4. Effect of hydrogen on Cr emission signal and signal-to-noise ratio. The plasma was operated at 800 W.

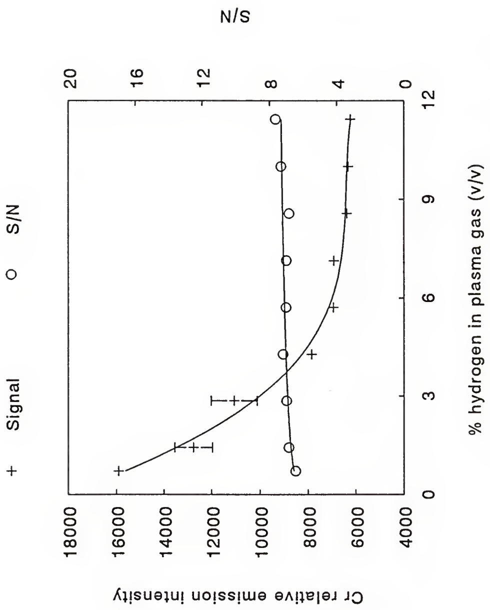
+ Signal
○ S/N
Cr relative emission intensity
18000
16000
14000
12000
10000
8000
6000
4000
S/N
20
16
12
8
4
0
% hydrogen in plasma gas (v/v)
0
3
6
9
12

Figure 3-5. Effect of hydrogen on As emission signal and signal-to-noise ratio. The As was introduced as AsH_3 and the plasma was operated at 500 W.

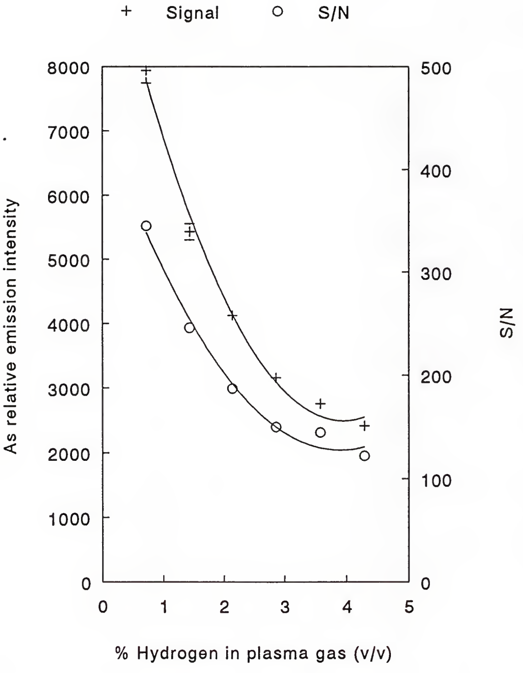
+ Signal
○ S/N
As relative emission intensity
8000
7000
6000
5000
4000
3000
2000
1000
0
500
400
300
200
100
0
S/N
0
1
2
3
4
5
% Hydrogen in plasma gas (v/v)

Figure 3-6. Effect of hydrogen on Hg emission signal and signal-to-noise ratio. The Hg was introduced as a vapor and the plasma was operated at 500 W.

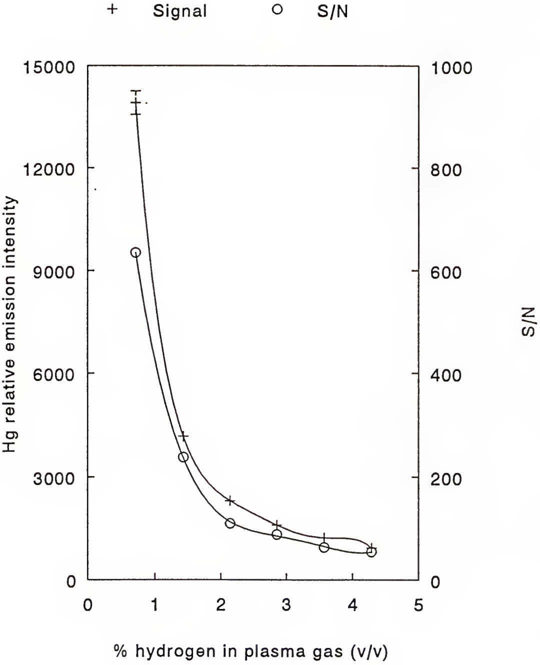
+ Signal
○ S/N
Hg relative emission intensity
15000
12000
9000
6000
3000
0
1000
800
600
400
200
0
S/N
0
1
2
3
4
5
% hydrogen in plasma gas (v/v)

Hg. In the case of Zn and Cu, solutions were introduced into the plasma by nebulization while direct introduction of AsH_3 gas and Hg vapor was utilized. In all cases the signal decreases with an increase in hydrogen concentration. This is probably the result of the decrease in electronic excitation temperature as the concentration of hydrogen is increased. Since T_{el} decreases with an increase in the hydrogen concentration, it is expected that the signal will also decrease. The signal-to-noise ratios, however, show different behavior for those elements introduced by nebulization compared to those introduced directly as gases. The S/N for Zn increases to a maximum at 4.5 % H_2 and then decreases rapidly. The S/N for Cr is almost constant regardless of the concentration of H_2. The S/N for both As and Hg decreases with an increase in hydrogen concentration.

The differences in the behavior of the two groups of elements can be explained in terms of what happens when the samples are introduced into the plasma. In the case of solution nebulization, the sample has to be vaporized, atomized, and excited. A high rotational temperature would enhance vaporization and atomization of the sample. Since the concentration of hydrogen has opposing effects on the T_{el} and T_{rot}, there is some compromise concentration of hydrogen that results in the optimum signal. It appears from the behavior of Cr that the effect of decrease in T_{el} is almost exactly offset by the increase in T_{rot} so that the S/N is almost independent of the hydrogen concentration.

For samples introduced as gases, the important parameter is the T_{el}. AsH_3 is easily decomposed at temperatures less than 800 ^{0}C. The T_{rot} of the plasma even without the addition of hydrogen is therefore sufficient to dissociate the AsH_3. Since T_{el} decreases with decrease in the concentration of H_2 in the plasma, the signal also decreases.

Summary

The amount of hydrogen in the plasma gas affects T_{el}, T_{rot}, and n_e. T_{el} decreases as the hydrogen concentration increases, T_{rot} and n_e increase as the hydrogen concentration increase. This results in different behavior for samples introduced into the plasma by solution nebulization (and hence require both T_{el} and T_{rot} to be high) and those samples introduced directly as gases requiring high T_{el}. In the former case, approximately 4.5 % of hydrogen was found to work well while in the later, the minimum amount of H_2 which would allow operation of the plasma was best.

CHAPTER 4
ANALYSIS OF ARSENIC AFTER HYDRIDE GENERATION

Introduction

The hydrides of As, Bi, Ge, Pb, Sb, Se, Sn, and Te are of importance for the determination of these elements because they are all volatile [102] (see Table 5-1). They can therefore be generated as gases suitable for effective sample introduction into atom reservoir or excitation sources for determination by AAS, AFS, or AES.

In this technique, aqueous sample solutions containing the analyte are acidified and treated with a reducing agent to generate the hydride of the analyte. The hydride is then swept out of the reaction vessel into the plasma where it is decomposed to the gaseous metal atoms, excited, and detected.

The advantages of utilizing this technique are as follows: (1) introduction of gases into plasmas is highly efficient compared with pneumatic nebulization. In pneumatic nebulization, 95% of the sample solution is discarded, whereas the transport efficiency of gases to the plasma can approach 100%; therefore more analyte reaches the plasma, resulting in better limits of detection; (2) the generated gas is separated from solution, eliminating matrix interferences on subsequent measurements; (3) the gases formed may be trapped in a balloon, cold trap, etc. and introduced into the plasma as a

Table 4-1. Boiling points of some covalently bonded hydrides of practical analytical importance [102].

Element	Hydride	Boiling point (^0C)
As	AsH_3	-62.5
Bi	BiH_3	-22
Ge	GeH_4	-88.5
Pb	PbH_4	-13
Sn	SbH_3	-18.4
Se	H_2Se	-41.3
Sn	SnH_4	-51.8
Te	H_2Te	-2.3

plug, thereby preconcentrating the sample; and (4) since the sample is introduced as a gas, the plasma does not have to desolvate and vaporize the sample. The role of the plasma is to dissociate the hydrides and excite the atoms. Low power plasmas can therefore be used.

Some of the disadvantages of this technique are that cumbersome and time comsuming procedures are used if collection devices such as balloons and cold traps are used and operational conditions may have to be optimized for each element or some groups of elements since their hydrides are not formed under the same conditions.

Very little work has been done [103-105] on the use of CMPs as detectors after hydride generation although CMPs have the potential of sensitive determinations.

Of the various methods of hydride generation [106,107], the acid-sodium borohydride ($NaBH_4$) reaction is the most frequently used because it is the most effective. The unbalanced reaction can be presented as [106,107]:

$$NaBH_4 + 3H_2O + HCl \rightarrow H_3BO_3 + NaCl + 8H$$

$$8H + E^{m+} \rightarrow EH_n + H_2 \text{ (excess)}$$

Where E is the analyte and m may or may not equal n.

Two approaches, continuous and batch, may be utilized to introduce the hydride into the plasma. In the continuous process, the reagents are continuously introduced into a mixing chamber where the reaction takes place. The gaseous products are swept into a gas-liquid separator where the liquid passes to a drain and the gas to the plasma. This has the advantage that the process can easily be automated. In the batch process, an aliquot of the acid solution containing the analyte is mixed with $NaBH_4$. The resulting hydrides (and gaseous byproducts) are swept into the plasma directly or as a plug after condensation in liquid N_2. Introduction after condensation in liquid N_2 has the advantage that H_2 produced as a byproduct of the reaction used to generate the hydrides can be vented away thereby reducing plasma instability resulting from the introduction of such high quantities of H_2. If a lot of hydrogen has to be passed into the plasma, high power levels have to be used. Also, preconcentration is achieved so that the limits of detection by this procedure tend to be superior.

All the hydride forming elements have poor limits of detection when determined directly by solution nebulization. Generation of the corresponding hydrides therefore allows determinations at lower concentrations. Use of the He CMP for excitation should result in more efficient excitation due to the higher ionization energy of the He.

Experimental

The system described in chapter 1 was used for the determination of arsine except that titanium electrodes (100% from Johnson Mattew, Ward Hill, MA) were used since graphite electrodes resulted in severe tailing of the As signals. The dimensions of the Ti electrodes were the same as the graphite ones. The final 3 mm of the Ti electrodes, however, were tapered as this resulted in better stability of the plasma.

Reagents

Deionized water was used throughout. The arsenic standard stock solution of 1000 ppm of As was prepared by dissolving 1.320 g reagent grade arsenic trioxide (As_2O_3) in H_2O containing 4 g NaOH and diluting to 1 L [108]. Dilute standard solutions were prepared daily from a 10 ppm As in 0.5% HCl standard prepared from the stock solution. 5% $NaBH_4$ in 0.11 M NaOH (for stabilizing the $NaBH_4$ [109] was prepared from 99% $NaBH_4$ and 99.99% NaOH both, supplied by Aldrich Chemical Company, Milwaukee, WI. This was prepared fresh every 4 hours.

Procedure for Measurement

The arsenic solution was added to a 100 mL reaction vessel (see Figure 4-1) and acidified with 25 mL of 1 M HCl. Other than connecting tubes which were made of Tygon tubing, the system (laboratory constructed) was made entirely of glass. Teflon was used as the transfer line from the AsH_3 trap to the plasma. $NaBH_4$ solution was then added (4 mL), via a septum, over a period of 2 minutes using a syringe pump. During the addition and the course of the reaction, He gas was passed to the sample tube of the torch through S3 at a flow rate of 60 cm^3/min. He was also bubbled through the reaction vessel. Stopcocks S1 and S2 are positioned so as to pass the

Figure 4-1. Schematic diagram of AsH_3 generation. S1 to S5 are stopcocks.

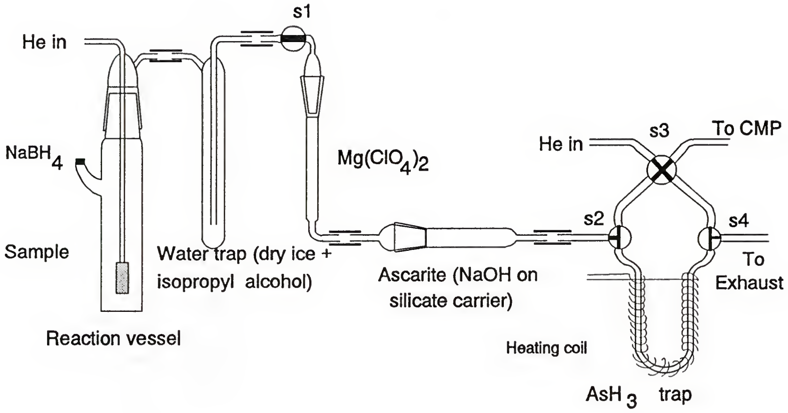
He in
s1
NaBH4
Sample
Reaction vessel
Water trap (dry ice + isopropyl alcohol)
Mg(ClO4)2
Ascarite (NaOH on silicate carrier)
He in
s3
To CMP
s2
s4
To Exhaust
Heating coil
AsH 3 trap

hydride through the AsH_3 trap. S4 was positioned so as to vent the hydrogen, produced during the reaction. The water trap was made from a mixture of isopropyl alcohol and dry ice (temperature of -40° C). Any remaining water was absorbed by the $Mg(ClO_4)_2$; CO_2 was absorbed by Ascarite (NaOH on a silicate base). When the reaction was judged complete (6 minutes), the helium to the reaction vessel was turned off, S2 and S3 were turned so that He passed through the AsH_3 trap, and S4 was turned so that the He was directed to the CMP. The liquid nitrogen flask was then removed and the AsH_3 trap heated using a Variac to vaporize the AsH_3 which was then swept to the CMP through the electrode.

The CMP plasma gas (98% He, 2% H_2) flow rate was 6 L/min and the optimum power was determined by measuring the signal and signal-to-noise ratio vs power. The optimum heating rate of the AsH_3 trap was also determined. Using the optimized conditions, the limit of detection and linear dynamic range for As were determined.

Results and Discussion

Figure 4-2 shows the transient signals for As (228.8 nm) and 235.0 nm. The 228.8 nm line was found to be most intense, and the 235.0 nm line was on top of a molecular band so that only the 228.8 nm line was used in this work. A cross-section on the diode corresponding to the As signal gives the signal with respect to time (Figure 4-3).

Figure 4-2. A 3-dimensional plot showing the signal of 30 ng As, diode number, and time.

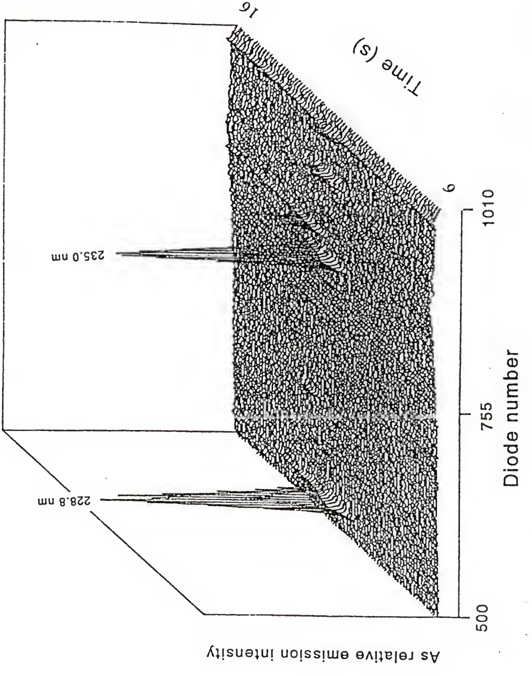
228.8 nm
235.0 nm
Time (s)
16
6
500
755
1010
Diode number
As relative emission intensity

Figure 4-3. Signal of 30 ng As vs time.

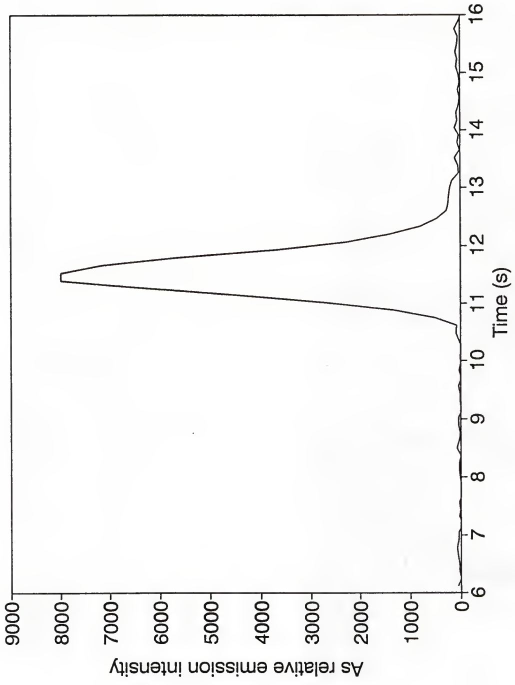
As relative emission intensity
0
1000
2000
3000
4000
5000
6000
7000
8000
9000
Time (s)
6
7
8
9
10
11
12
13
14
15
16

Optimum Heating Rate of the AsH_3 Trap

Figure 4-4 shows the signals obtained when the AsH_3 trap was heated at different rates. The following effects were observed. (1) The time of appearance of the signal (from the time the heating coil is turned on) decreases as the heating rate increases (Figure 4-5a). Increasing the heating rate reduces the time required to raise the temperature of the heating trap to the level where the AsH_3 is volatilized. When no heating was done the signal appeared after 37 s, whereas only 10s were required for 243 W and 370 W. (2) The signal duration (peak width at base, in seconds) also decreased as the heating rate was increased. The signal duration when no heat was applied to the AsH_3 trap was 16 s while the duration for 58 W - 370 W was 4 s (Figure 4-5b). The higher heating rates allow the sample to be volatilized quickly from the AsH_3 trap. (3) Peak height increases rapidly as the heating rate increases (Figure 4-5c). Since the higher heating rates volatilized the sample quickly, the sample was introduced to the plasma as a more concentrated "plug" resulting in the higher signals. The peak height for 243 W and 370 W were, however, almost the same, indicating that the AsH_3 was being volatilized as fast as it could be. Increasing the heating rate beyond this point does not increase the signals any further but may risk decomposition of the AsH_3 in the AsH_3 trap. All subsequent work was therefore done at 243 W.

Figure 4-4. Signals of As resulting from different heating rates of AsH_3 trap..

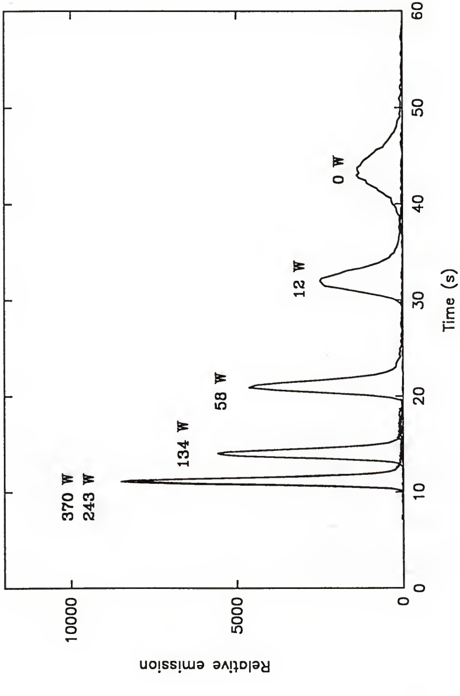
Relative emission
0
5000
10000
Time (s)
0
10
20
30
40
50
60
370 W
243 W
134 W
58 W
12 W
0 W

Figure 4-5. Effect of power across heating coil on (a) time of appearance of signal (elapse time) (b) signal duration and (c) peak height.

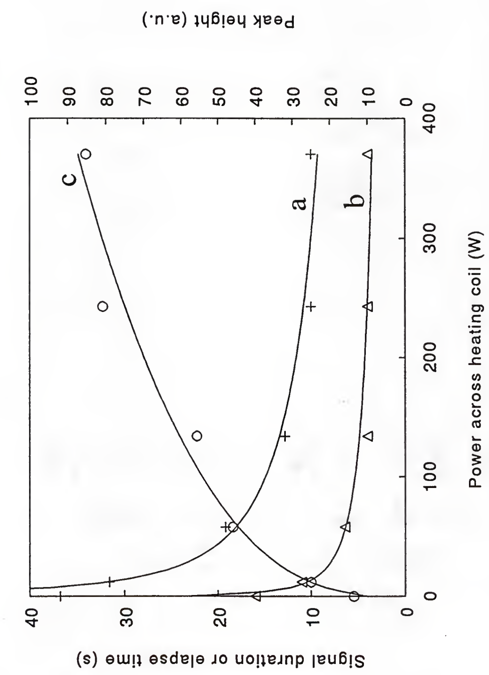
Signal duration or elapse time (s)
0
10
20
30
40
Peak height (a.u.)
0
10
20
30
40
50
60
70
80
90
100
Power across heating coil (W)
0
100
200
300
400
a
b
c

Effect of Power

The As signal increased as the power was increased, but the S/N was constant after 300 W (figure 4-6). As the power is increased, more energy is available to excite the As (both excitation and rotational energy increase with power), and therefore the signal increases. The noise however increased with power resulting in constant S/N ratios. There is therefore no advantage to working at high power levels and 500 W was used throughout.

Limit of Detection and Linear Dynamic Range

Figure 4-7 shows the log-log plot of the signals (peak area) versus the concentration from the LOD to 3000 ng. The slope of the plot was 0.951 with a linear dynamic range greater than 10^4 and $R^2 = 0.999$. Using a calibration curve from 10 ng to 300 ng, a linear plot of signal versus concentration was obtained. The limit of detection (3σ) was determined to be 0.03 ng. This corresponds to a concentration LOD of 0.4 pg/mL for a 75 mL sample.

Summary

Arsenic was determined with an absolute LOD of 0.03 ng corresponding to concentration LOD of 0.06 pg/mL and 0.04 pg/mL for 50 mL and 75 mL sample volumes, respectively. The LDR was found to be greater than 10^4 which is typical of atomic emission techniques. This work also shows the importance of optimizing the AsH_3 heating rate in order to obtain high sensitivity and reproducible peak heights.

Figure 4-6. Effect of power on signal and signal-to-noise ratio.

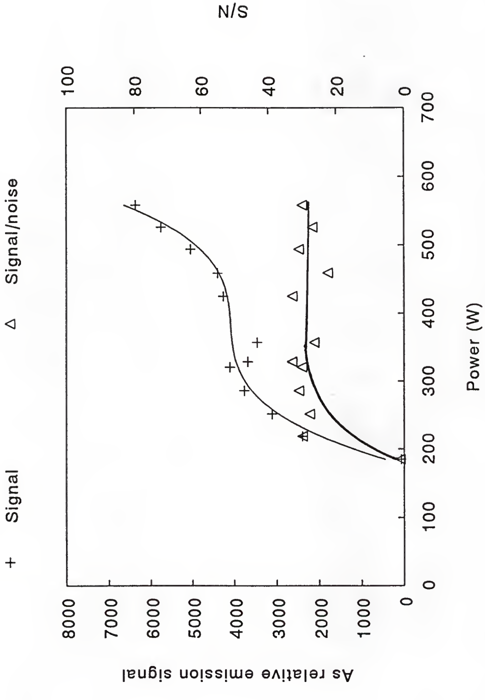
+ Signal
Δ Signal/noise
As relative emission signal
8000
7000
6000
5000
4000
3000
2000
1000
0
S/N
100
80
60
40
20
0
0
100
200
300
400
500
600
700
Power (W)

Figure 4-7. Log-log plot of As signal vs amount of As.

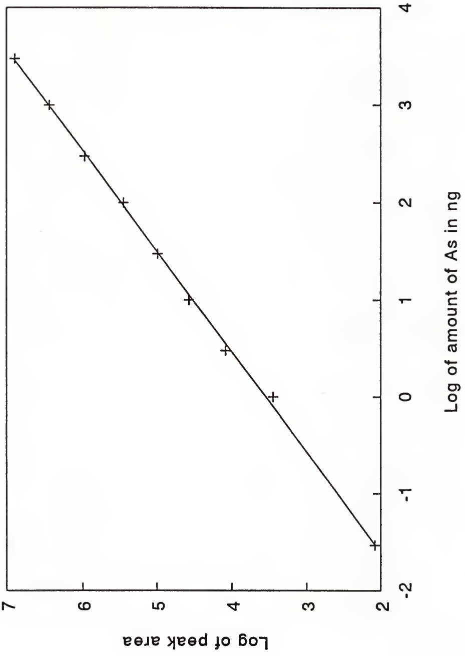
Log of peak area
7
6
5
4
3
2
-2
-1
0
1
2
3
4
Log of amount of As in ng

An attempt was made to determine Hg and Se using a similar technique. It was found that Hg condensed on the transfer line and/or electrode. In order to use this technique for Hg, it may be necessary to heat the transfer line to the CMP and find an electrode material to which mercury does not adsorb. Using the same instrumentation for Se resulted in poor reproducibility. Use of Chromosorb 102 [108] instead of NaOH to absorb CO_2 should allow the determination of Se.

CHAPTER 5
ANALYSIS BY SOLUTION NEBULIZATION

Introduction

Solution introduction is by far the most common means of sample introduction in flame spectroscopy and ICP spectroscopy. This is because solutions may be introduced into the plasma or flame rapidly utilizing simpler systems compared to solids. Solution analysis also result in better precision.

Aerosols provide the easiest means of introducing liquids into plasmas. Generally this is accomplished by either pneumatic nebulization, which is by far the most common, or by ultrasonic nebulization. Because of the low power levels employed by most MIPs e.g. [11,12], direct introduction of solutions could not be accomplished, especially for earlier systems, in most cases, due to the low tolerance of such low power plasmas to the introduction of molecular species.

Due to the high power level employed in this work, no problems associated with solution introduction by nebulization were encountered. Also, in CMPs, the plasma is anchored on the electrode, making it more tolerant to sample introduction disturbances. Limits of detection of some elements, the effect of power on Cr, Mn and Al signals, and the matrix effects of PO_4^{3-} and Na^+ on Ca emission signals were evaluated.

Experimental

All solutions were prepared from commercial atomic absorption standards (Fisher Scientific Co., Fair Lawn, NJ or Inorganic Ventures, Inc., Brick, NJ). The solutions were pumped to the nebulizer (Meinhard) using a Rabbit peristaltic pump (Rainin Instrument Co., Boston MA). In this work, no solution desolvation was used. Unless otherwise specified, a power level of 800 W was used throughout. The spectrometer and photodiode array spectrometer described in Chapter 1 were used. After data acquisition, a different program from that supplied with the photodiode array detector called SIDE, (D. Hueber, unpublished work) was used. This program allowed the signals at two diodes to be displayed for all the spectra acquired; the mean of the difference between the two diodes to obtain the signal with background correction, the mean and standard deviation of each diode, and the standard deviation of the difference between the two diodes were all calculated. This allowed faster data acquisition than the original OSMA program controlling the photodiode array.

Matrix effects were investigated by measuring the Ca emission signals in the presence of varying amounts of PO_4^{3-} and Na.

Results and Discussion

Effect of Various Parameters on Cr Emission

Various parameters were optimized for Cr emission. Measurement of Cr signals across the plasma 5 mm above the electrode (radial profiles) showed a maximum Cr signal at 1 mm from the center of the plasma. Most of the signal was observed within a total distance of 3 mm (approximately 1.5 mm from the center on each side). Outside this distance, very small Cr signals are observed for the 10 ppm standard employed, indicating the sample is concentrated around the center of the plasma; no temperature changes were observed across the plasma (Chapter 2). The Cr signal also showed a maximum at 6 mm above the electrode tip, with signals observable from 4 mm above the electrode top to 11 mm above the electrode top. Low or no signals are observed near the electrode. The area near the electrode is at low temperature. Since the plasma is formed on the outer surface of the electrode, the center of the electrode would therefore be expected to be cooler, leading to the reduction of any observed signals. Rotational temperature measurements (see chapter 2) confirm this with T_{rot} increasing to about 4 mm above the electrode top before decreasing. Optimization of He carrier gas flow rate showed a maximum Cr signal at 650 cm^3/min for a solution flow rate of 2.2 mL/min. It appears that below this flow rate, the signal is limited by the amount of sample reaching the plasma, while above it, too much sample is introduced into the plasma for efficient desolvation and excitation.

Figure 5-1 shows the effect of solution flow rate on the Cr signal and signal-to-noise ratio with the carrier gas flow rate held constant at 650 cm^3/min. The signal increased to a

Figure 5-1. Effect of solution uptake rate on Cr emission (+) and signal-to-noise ratio (o).

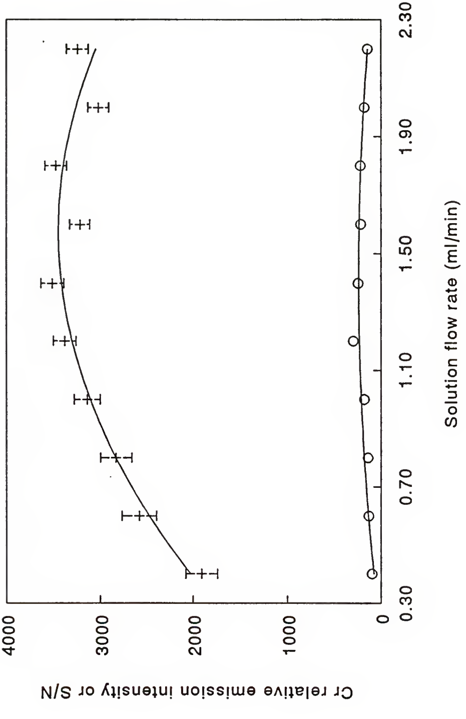
Cr relative emission intensity or S/N
0
1000
2000
3000
4000
Solution flow rate (ml/min)
0.30
0.70
1.10
1.50
1.90
2.30

flow rate of 1.4 mL/min and then decreased. The same pattern is observed for the effect of solution flow rate on electron number density (Chapter 2). This effect might be attributed to the same factor as for the carrier gas flow rate. At constant carrier gas flow rate, the amount of water entering the plasma increases as the solution pump flow rate is increased. A point is reached where more solution is introduced into the plasma than can be efficiently excited. The solution flow rate is therefore set constant at 1.4 mL/min, with carrier gas flow rate of 650 cm^3/min for all subsequent work.

Effect of Power

The effect of power on the signals and signal-to-noise ratios of Cr, Mn, and Al are shown in Figures 5-2 to 5-4. In all cases there is a sharp increase of the signals as the power is increased. The signal to noise ratios also increase continuously over the power levels investigated. This indicates that power levels greater than 1000 W would improve sensitivities and limits of detection of these elements. Unfortunately, the electrode needed replacing more often (at least twice a day) at power levels greater than 800 W. A power level of 800 W was therefore used in all the subsequent work.

Limits of Detection

Table 5-1 shows the limits of detection, defined as the concentration of analyte element which will produce a net analyte signal the magnitude of which is a factor of three times the standard deviation of the background, for several

Figure 5-2. Effect of microwave power on Cr emission (+) and signal-to-noise ratio (o).

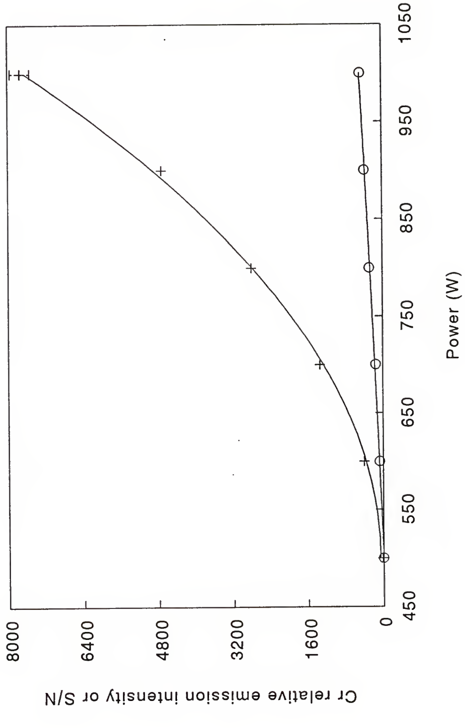
Cr relative emission intensity or S/N
8000
6400
4800
3200
1600
0
450
550
650
750
850
950
1050
Power (W)

Figure 5-3. Effect of power on Mn emission (+) and signal-to-noise ratio (o).

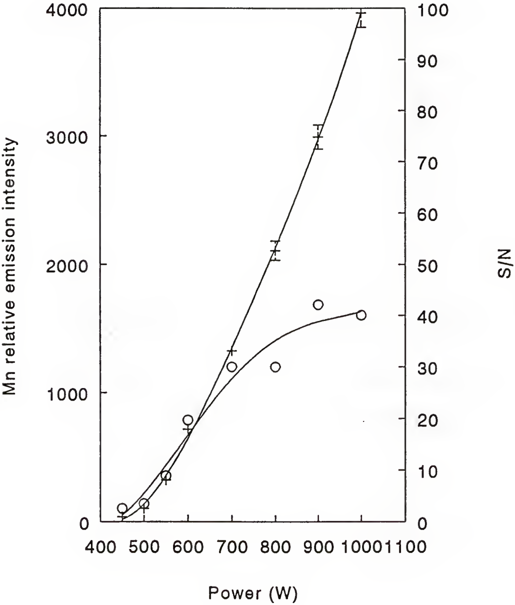
4000
3000
2000
1000
0
Mn relative emission intensity
100
90
80
70
60
50
40
30
20
10
0
S/N
400
500
600
700
800
900
1000
1100
Power (W)

Figure 5-4. Effect of power on Al emission (+) and signal-to-noise ratio (o).

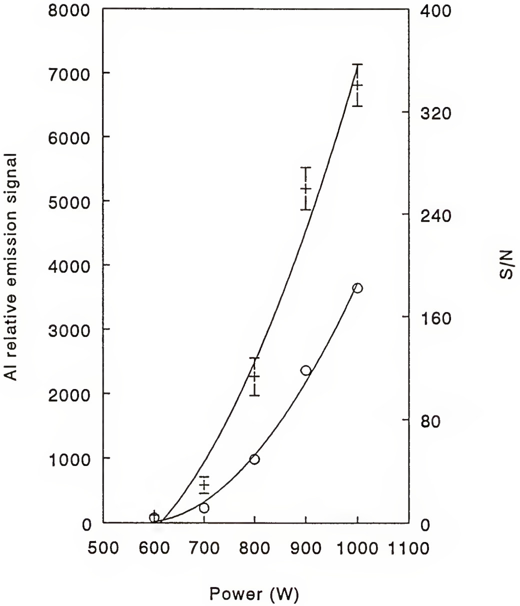
8000
7000
6000
5000
4000
3000
2000
1000
0
Al relative emission signal
400
320
240
160
80
0
S/N
500
600
700
800
900
1000
1100
Power (W)

Table 5-1. Limits of detection ($\mu g/mL$) for several elements determined by solution nebulization into CMP and ICP.

	Wavelength (nm)	This work*	Ref. 48	Ref. 49	Ref. 19	Ref. 110
Al	396.15	0.3	0.5	0.003	0.3	0.02
Mn	403.08	0.1	-	-	0.05	0.001
Cu	324.75	0.08	-	-	0.04	0.005
Cr	425.43	0.05	-	0.009	0.04	0.006
Li	670.78	0.004	0.005	-	0.7	0.9
Sr	460.73	0.05	0.08	-	0.04	0.0004
K	766.49	0.02	0.26	-	0.04	-
Na	589.59	0.01	0.01	0.00005	0.03	0.03
Sn	303.41	0.1	-	0.01	1.8	0.1
Zn	481.05	0.1	5	-	0.2	0.002

* LODs defined as concentration in ppm resulting in a signal of three times the standard deviation of blanks. The wavelengths are those used in this work.

elements obtained in this work. Those obtained by CMP-OES and ICP-OES by other workers [19,48,49,110] are also given for comparison purposes. This work gives limits of detection comparable to those by those workers where molecular plasmas were employed [19,48]. In refs. [19] and [48] pure nitrogen plasmas were employed at a power level of about 400 W. The limits of detection in ref. [19], however, are defined as the concentration of the analyte element which will produce a net analyte signal the magnitude of which is a factor of two times the standard deviation of the background signal. The limits of detection in ref. [48] were with desolvation of the aerosol. Those from ref. [48] and ref. [49] are defined as in this work. The LODs obtained in ref. 49 were for a pure He plasma operated at 900 W. These are superior compared to those obtained in this work and actually compare favorably to those obtained by Ar-ICP [110].

The limits of detection obtained in this work were inferior to those obtained by Ar-ICP or pure He-CMP operated at 900 W. As the power dependency of Cr, Mn, and Al shows, operation of this type of plasma at even higher power levels should improve the limits of detection.

Matrix Interferences

The influence of phosphate on the signal from Ca is a classical example of compound formation in the condensed phase in the flame [111-113]. This effect disappears in C_2H_2-N_2O flame or after the addition of a releasing agent [114-116].

The reduced extent of this interference in the ICP has been used to demonstrate the superiority of the ICP over flames for analytical applications [117].

The effect of an easily ionizable element (EIE) in flame spectroscopy has been well characterized. Enhancements in emission intensity from atom lines is observed when signals with and without the presence of an EIE are compared [112,118]. These observations have been rationalized on the basis of the shift in the ionization equilibrium for the analyte atom (x), ion (x^+) and electron (e^-)

$$x \rightleftharpoons x^+ + e^-$$

The addition of the EIE has the effect of increasing the electron density in flames such that the equilibrium is shifted towards the neutral atom species causing enhancement of the neutral line emission [113,119].

The situation is not quite so well defined in the ICP, partially because of the variability in plasma operation conditions between investigators and partially because the influence of EIE has been observed to be complex in nature. Koirtyohann et al. observed slight enhancements of Ca atom line emission in the presence of an EIE up to 10 mm above the load coil, an increased enhancement of the signal between 10 mm and 15 mm above the load coil and then almost no effect above 15 mm [120]. Larson et al. [121] observed enhancement of Ca atom emission, the magnitude of which increased with increase in molar ratio of Na to Ca. The enhancements also increased with increasing height above the load coil. Enhancement of atomic Ca emission signal was also observed by Abdalla et al. [122], and Kawaguchi et al. [123].

Figure 5-5 shows the effect of PO_4^{3-} on a 20 ppm Ca emission signal. There was no effect on the signal by the PO_4^{3-} below 100 ppm, but some suppression above 100 ppm. This shows some matrix interference on the Ca signal when the concentration of the PO_4^{3-} in the sample is high enough. A similar type of interference was observed in the ICP by Larson et al. [121]. Figure 5-6 shows the effect of Na on Ca emission. Within this concentration range, very little enhancement is observed.

Summary

Optimization of various parameters is required in order to obtain the most sensitivity and the best limits of detection in CMP. In this work, this has been shown by optimizations carried out for Cr by varying the solution flow rate, carrier gas flow rate, and power. Limits of detection evaluated under compromise conditions compared well with molecular gas CMPs but were inferior to those obtained by Ar-ICP or pure He-CMP operated at 900 W. Improved limits of detection should be realized if power levels higher than the 800 W utilized in this work are used.

Figure 5-5. Effect of PO_4^{3-} on Ca emission signal.

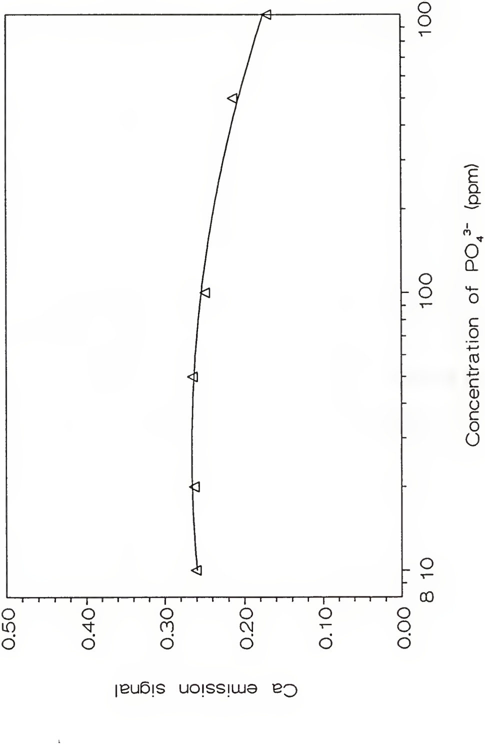
0.50
0.40
0.30
0.20
0.10
0.00
Ca emission signal
8
10
100
1000
Concentration of PO_4^{3-} (ppm)

Figure 5-6. Effect of Na^+ on Ca emission signal.

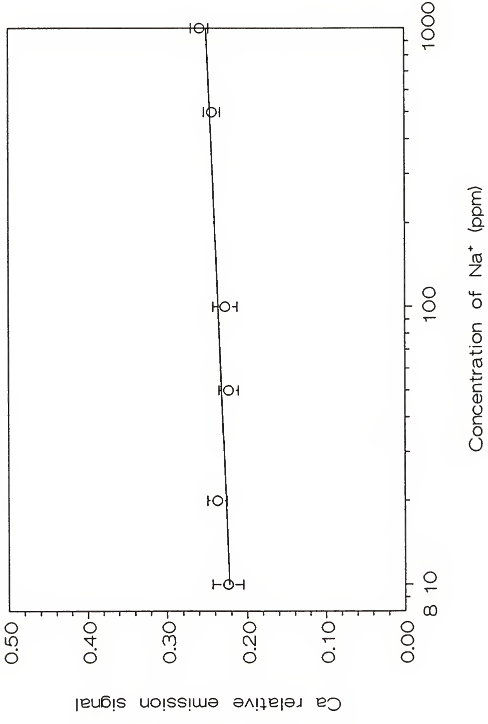
Ca relative emission signal
0.00
0.10
0.20
0.30
0.40
0.50
8
10
100
1000
Concentration of Na$^+$ (ppm)

CHAPTER SIX
ANALYSIS OF STEEL BY DIRECT SAMPLE INJECTION

Introduction

Since the first reports by Salin and Horlick [124] and Sommer and Ohls [125], the direct insertion of samples into the ICP has shown promise for the determination of trace and ultra trace elements [124-132]. The publication by Karanassios and Horlick [127] discusses the development in direct solid insertion (DSI) into ICPs. In fact DSI, is one group of sample introduction techniques for direct analysis of solids. Other methods of introducing samples directly include powder entrainment [133], slurries [134], ablation techniques [135] and electrothermal atomizers [136,137].

The direct analysis of solids is important for several reasons. Dissolution of solids may require use of hazardous chemicals (e.g., use of HF in silicate analysis) and is, in most cases, time consuming. Fusion techniques result in solutions of high salt content, with potential for clogging nebulizers. Sample dissolution also results in dilution of the sample, resulting in poor limits of detection when considering the amount of analyte that can be determined in the original sample. Degradation of plasma performance as an excitation and atomization cell may also be observed owing to the introduction of solvent (together with the analyte). There is potential for contamination from reagents used to dissolve the sample, and some volatile elements may be lost during the dissolution process. Introduction of solutions to the ICP is very inefficient since less than 5% of the sample make it to the plasma, the rest being rejected by the spray chamber as waste. These problems are avoided by direct sample introduction. Direct sample introduction into plasmas, however, poses some problems. Poorer precision than with solution nebulization is usually observed [138]. Moreover, calibration curves are difficult to determine especially if compared to solution determination where aqueous standards (usually prepared by dissolving a salt in dilute acid) can be used directly. In some cases, matrix modification in the condensed or aqueous phase may minimize chemical interferences. Application of chemical modification to solid samples have been done in DSI-ICP [139-142]. Direct analysis of conducting samples by radio frequency (RF) sputtering RF capacitively coupled plasma has been described by Liang and Blades [143].

Until recently, no work on direct solid sampling methods without analyte vapor transport had been developed for microwave plasmas. Ali et al. [46] developed a method where dry tomato leaf samples and coal fly ash samples (sometimes diluted with graphite) were deposited in a graphite cup. The graphite cup fit into a hollow graphite electrode. The sample was then ashed in situ and emission signals observed at 400 W for tomato leaves and 700 W for coal fly ash. Limits of detection that were determined were in the ng range.

In this work, a similar technique is used for the analysis of steel samples.

Experimental

The metal sample to be analyzed was machined into a cylinder which could fit tightly into a hollow graphite electrode in order to provide electrical contact (Figure 6-1). The plasma gas (94.5% He, 4.5 % H_2) flow rate was kept at 6 L/min. No carrier gas was used. In fact, the hollow cathode did not have a hole though it. The plasma was ignited and the power adjusted. The signal was recorded after five minutes in order to allow it to stabilize. Calibration curves were obtained by using steel samples of known composition (NIST SRM 442-450).

Results and Discussion

Figure 6-2 shows the effect of power on Cr, Mn, and Cu signals. In all cases, negligible signals are observed at power levels less than 350 W. At power levels less than 350 W, the plasma is not energetic enough to vaporize the sample. The signals increase sharply as the power is increased as the result of more excitation energy being available to excite the sample that is introduced into the plasma. Measurements are only carried out to 500 W because some samples begun to melt at power levels greater than 500 W. This raises an interesting question as to whether the sample is thermally vaporized or

Figure 6-1. The graphite electrode (a) and sample (b) for solid sampling into CMP. Dimensions are in mm.

a

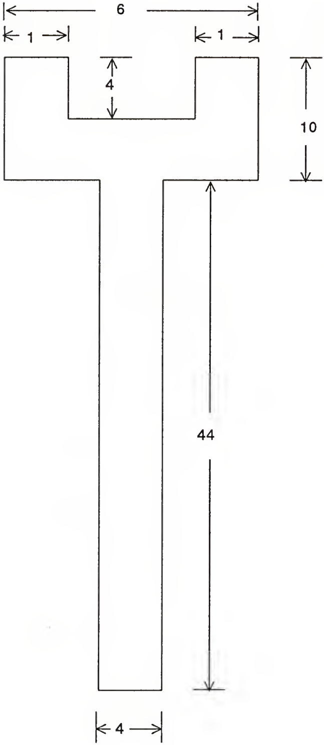

b

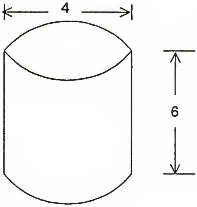

Figure 6-2. Effect of power on the emission signals of Cr, Mn, and Cu.

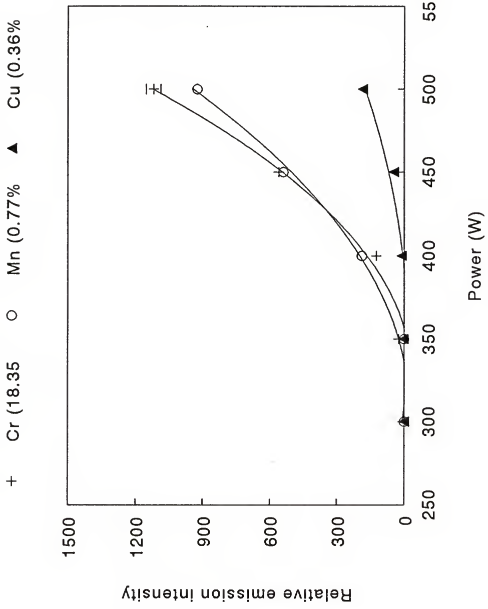
+ Cr (18.35
○ Mn (0.77%
▲ Cu (0.36%
Relative emission intensity
0
300
600
900
1200
1500
Power (W)
250
300
350
400
450
500
550

some other mechanism is responsible for the introduction of the sample material from the electrode into the plasma. Figures 6-3 to 6-6 show calibration curves for Mn, Cr, Pb, and Sn. In all cases, linear calibration curves were obtained. Each point is the mean of 20 measurements and the error bars correspond to one standard deviation. In the cases where error bars do not appear, the standard deviation was too small to appear on the graph. Since the calibration curves were determined by using steel samples of different composition, the method should be applicable for the analysis of steels. Those elements at high concentration Mn, and Cr show poor precisions and larger deviations from the line than those at low concentration (Pb and Sn). Interference filters are used in the cases where the signals are too high to be detected directly by the photodiode array. The calibration curves, especially at high analyte concentrations, do not pass through the origin when linear regression is used. This is probably due to inadequate background correction of the complex spectra obtained. Limits of detection for Pb and Sn were determined to be 0.08 μg/g and 5 μg/g respectively. These limits of detection compare well with those obtained by DSI-ICP. Using the 220.3 nm Pb line, Abdullah and Haraguchi [144] determined a limit of detection of 1.40 μg/g, Shao and Horlick [130] determined a limit of detection of 0.33 ppm and McLeod et al. [128] determined a limit of detection of 0.08 μg/g. Using the 283.3 nm Pb line, Page et al. [145] determined a limit of

Figure 6-3. Calibration curve for Mn by solid sample introduction.

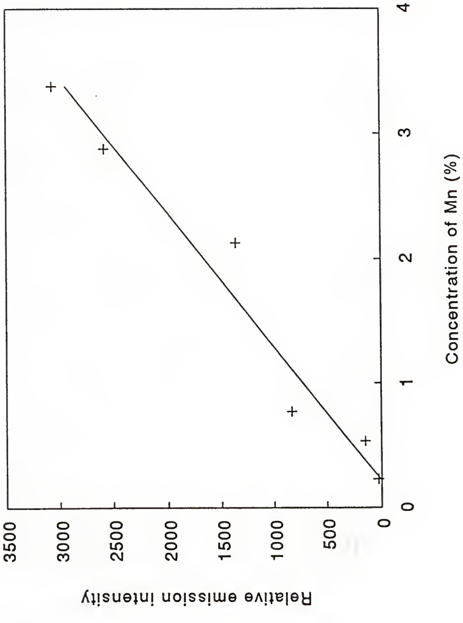
Relative emission intensity
0
500
1000
1500
2000
2500
3000
3500
Concentration of Mn (%)
0
1
2
3
4

Figure 6-4. Calibration curve for Cr by solid sample introduction.

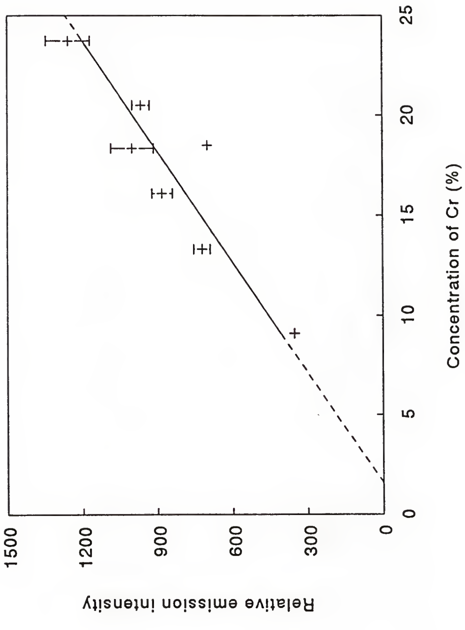
Relative emission intensity
0
300
600
900
1200
1500
Concentration of Cr (%)
0
5
10
15
20
25

Figure 6-5. Calibration curve for Pb by solid sample introduction.

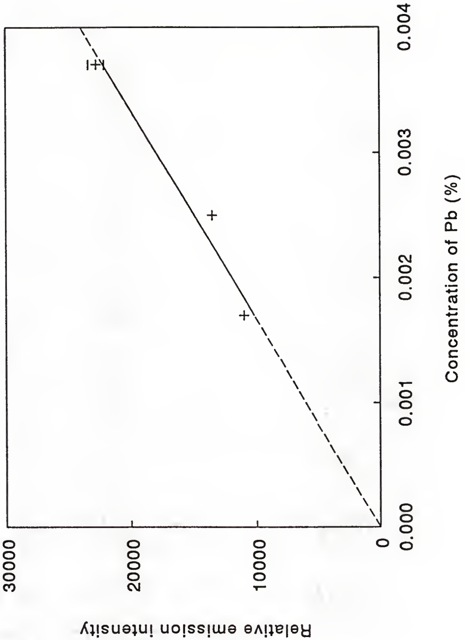
Relative emission intensity
0
10000
20000
30000
0.000
0.001
0.002
0.003
0.004
Concentration of Pb (%)

Figure 6-6. Calibration curve for Sn by solid sample introduction.

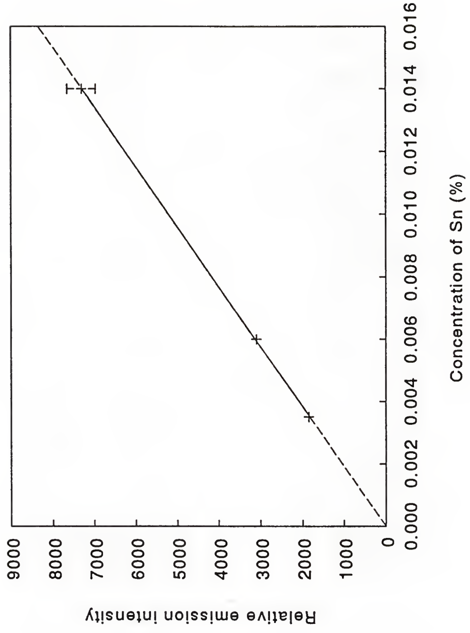
Relative emission intensity
9000
8000
7000
6000
5000
4000
3000
2000
1000
0
0.000
0.002
0.004
0.006
0.008
0.010
0.012
0.014
0.016
Concentration of Sn (%)

detection of 1.3 ppm. Abdulla and Haraguchi [144] and Shao and Horlick [130] determined limits of detection of 1.25 μg/g and 0.06 ppm, respectively, for Sn using the 189.9 nm line.

Summary

A method for the direct analysis of metal samples has been outlined. The only requirement was a hollow electrode and the sample shaped in the form of a cylinder. Limits of detection obtained by this technique show possible determinations of constituents in steel from less than 1 μg/g to the percent range, and linear calibration curves were obtained. This method has the advantage over direct sample introduction of powder samples in that a steady state signal is obtained. Use of the photodiode array detection system allowed background correction.

CHAPTER SEVEN
CONCLUSIONS AND FUTURE WORK

Depending on the plasma conditions, electronic excitation temperatures are determined to lie between 2000 K and 5000 K, rotational temperatures are between 1800 K and 3000 K, and electron number densities varied between $4x10^{14}$ cm^{-3} and $9x10^{14}$ cm^{-3}. These values are comparable to those observed by other workers for He plasmas. An excellent limit of detection of 0.03 ng for arsenic (after hydride generation) is determined. This corresponds to a concentration limit of detection of 0.4 pg/ml if a 75 mL sample is used. Limits of detection determined by solution nebulization are in the sub ppm range. Very little interference of Na on the emission of a 20 ppm Ca solution is observed for Na concentrations up to 1000 ppm. A slight depression of a 20 ppm Ca signal is observed at PO_4^{3-} concentrations above 100 ppm. Direct introduction of metal samples resulted in linear calibration curves with limits of detection of 0.08 and 5 μg/g for Pb and Sn, respectively.

The capacitively coupled microwave plasma is a surprisingly under-utilized source even though it has potential for analysis of gas, liquid and solid samples. Future work that could be considered a direct extension of this work includes the following: (i) An extensive evaluation of different torches should be done in order to determine the best torch for this CMP. In this work, a 2 tube torch is used. A 3 tube torch might result in better stability of the plasma and a reduction of air entrainment. Torch dimensions giving the best plasma performance need to be determined. (ii) Different electrode materials and shapes need to be evaluated as well. During the work on hydride generation, tapered titanium electrodes resulted in a more stable plasma than flat ones. Memory effects of the graphite electrodes (observed with As determination after hydride generation) may be reduced by using pyrolytic graphite or glassy carbon. (iii) Most of this work was carried out between 700 W and 800 W in order to ensure a reasonable life of the electrodes. Using higher power, perhaps at the expense of higher flow rates, might result in lower limits of detection, since the plasma volume might be large enough for efficient desolvation of aerosols, atomization and excitation. Coupled with this, use of a desolvation system or ultrasonic nebulization should improve the limits of detection. (iv) Introduction of organic solvents into the CMP has not been attempted. Using a high power CMP should result in possible analysis in organic solvents.

A slight modification of the present system should allow operation based on the same principles as this work but without the need for the plasma to reside on the electrode. Figure 7-1 shows such an arrangement. A waveguide with a height slightly greater than $\lambda_g/4$ is used. The magnetron is

Figure 7-1. Sketch diagram of a microwave plasma where the plasma is not in contact with the electrode.

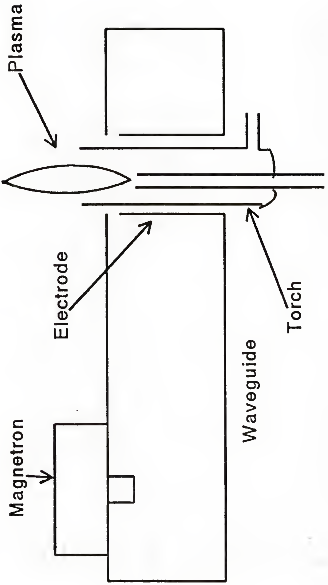
Plasma
Electrode
Torch
Waveguide
Magnetron

placed at a position $\lambda_g/4$ or an odd multiple from one of the ends and a cylindrical hollow "electrode" is placed at an odd multiple of $\lambda_g/4$ from the other end. The height of the electrode is selected to be $\lambda_g/4$. The waveguide height is chosen such that the electrode ends just before the waveguide. A torch is placed inside the electrode in such a way that the position where the plasma is to be formed coincides with the top of the electrode. Microwaves from the waveguide should be capacitively coupled to the end of the electrode and a plasma initiated inside the torch by a tesla coil. This method results in a microwave plasma that does not reside on an electrode and therefore will have the potential for operation at even higher power levels than used in this work. Some MIPs which are somewhat related to the system described above have been described [146-148].

APPENDIX
SPECTRA OF SOME ELEMENTS OBTAINED BY SOLUTION NEBULIZATION.

Figure A-1. Spectrum showing Cr emission lines.

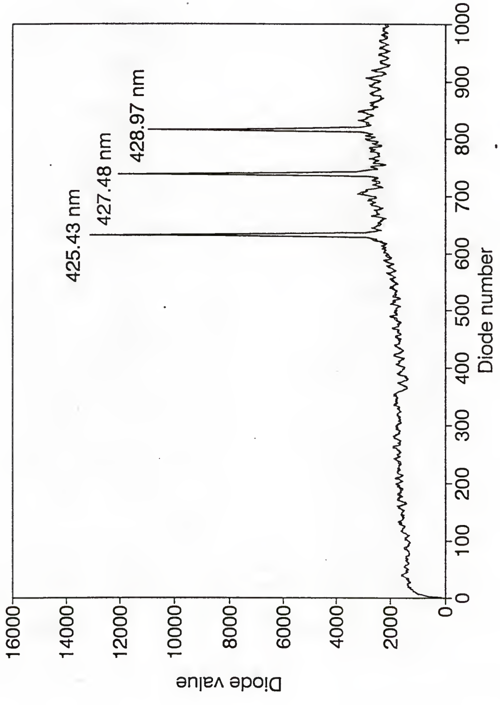
Diode value
16000
14000
12000
10000
8000
6000
4000
2000
0
Diode number
0
100
200
300
400
500
600
700
800
900
1000
425.43 nm
427.48 nm
428.97 nm

Figure A-2. Spectrum showing Mn emission lines.

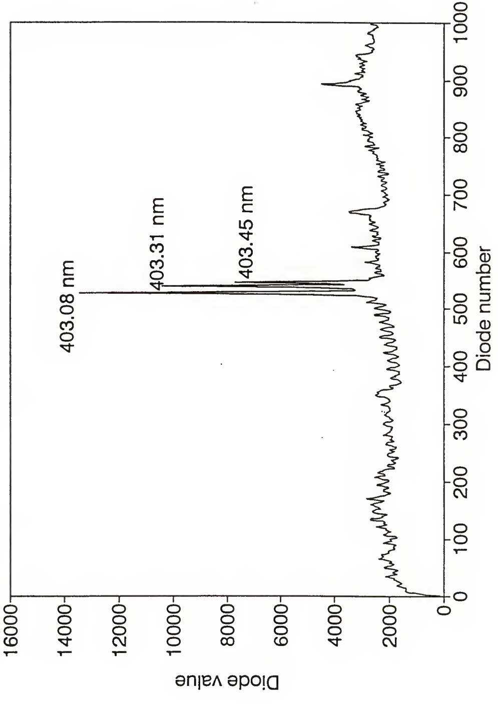
403.08 nm
403.31 nm
403.45 nm
Diode value
0
2000
4000
6000
8000
10000
12000
14000
16000
Diode number
0
100
200
300
400
500
600
700
800
900
1000

REFERENCES

1 C.I.M. Beenaker, *Spectrochim. Acta* **31B,** 483 (1976).

2 S. Greenfield, H. M. McGeachin, and P.B. Smith, *Talanta* **22**, 553 (1975).

3 P.C. Uden, *Trends Anal. Chem.* **6**, 238 (1987).

4 K.C. Ng and W.L. Shen, *Anal. Chem.* **58**, 2084 (1986).

5 J.W. Carnahan, *Am. Lab.* **15**, 31 (1983).

6 A.T. Zander and G.M. Hieftje, *Appl. Spectrosc.* **35**, 357 (1981).

7 S.R. Goode and K.W. Baghamann, *Appl. Spectrosc.* **38**, 755 (1984).

8 H.P. Broida and M.W. Chapman, *Anal. Chem.* **30**, 2049 (1958).

9 R.K. Skogeboe and G.N. Coleman, *Anal. Chem.* **48**, 611A (1976).

10 D.L. Haas and J.A. Caruso, *Anal. Chem.* **56**, 2014 (1984).

11 A.J. MacCormack, S.C. Tong, and W.D. Cooke, *Anal. Chem.* **37**, 1470 (1965).

12 C.A. Bache and D.J. Lisk, *Anal. Chem.* **37**, 1477 (1965).

13 J.H. Runnels and J.H. Gibson, *Anal. Chem.* **39**, 1398 (1967).

14 G.D. Critescu and R. Grigorovici, *Bull. Soc. Roum. Phys.* **42**, 37 (1941).

15 G.D. Critescu and R. Grigorovici, *Opt. Spektrosck.* **6**, 129 (1959).

16 G.D. Critescu and R. Grigorovici, *Naturwissenscaften* **29**, 571 (1941).

17 A.L. Stolov, *Uch. Zap. Kazan. Gos. Univ.* **116**, 118 (1956).

18 E. Badarau, M. Giurgea, G.H. Giurgea, and A.T. H. Trutia, *Spectrochim. Acta* **11**, 441 (1957).

19 J. Dahmen, *ICP Inf. Newsl.* **6**, 576 (1981).

20 J. Dahmen, *ICP Inf. Newsl.* **15**, 249 (1989).

21 Y. Asami and T. Hori, *Nature* **144**, 981 (1939).

22 M.A. Biondi, *El. Eng.* 806 (1950).

23 I.D. Cobine and D.A. Wilbur, *J. Appl. Phys.* **22**, 835 (1951).

24 R. Mavrodineanu and R.C. Hughes, *Development in Appl. Spectrosc.* **3**, 305 (1964).

25 R. Mavrodineanu and R.C. Hughes, *Spectrochim. Acta* **19**, 1309 (1963).

26 U. Jecht and W. Kessler, *Z. Anal. Chem.*, **198**, 27 (1963).

27 W. Kessler and F. Gebhardt, *Glastech. Ber.* **40**, 194 (1967).

28 W. Kessler, *Glastech. Ber.* **44**, 479 (1971).

29 M. Yamamoto and S. Murayama *Spectrochim. Acta* **23A**, 773 (1967).

30 S. Murayama, *Spectrochim. Acta* **25B**, 191 (1970).

31 S. Murayama, *J. Appl. Phys.* **39**, 5478 (1968).

32 S. Murayama, *Bunko Kenkyu* **19**, 237 (1970).

33 S. Murayama, H. Matsumo, and M. Yamamoto, *Spectrochim. Acta* **23B**, 513 (1968).

34 H. Goto, K. Kirokawa and M. Suzuki, *Z. Anal. Chem.* **225**, 130 (1967).

35 P.W.J.M. Boumans, *Plasma Sources other than Inductively Coupled Plasmas,* Ch. 2 in *Inductively Coupled Plasma Emission Spectroscopy-Part 1*. P.W.J.M. Boumans, Ed. John Wiley and Sons, New York (1987).

36 K. Govindaraju, G. Mevelle, and C. Chonard, *Anal. Chem.* **48**, 1325 (1976).

37 J.O. Burman and K. Bostrom, *Anal. Chem.* **51**, 516 (1979).

38 G.F. Larson and V.A. Fassel, *Anal. Chem.* **48**, 1161 (1976).

39 P.W.J.M. Boumans, F.J. de Boer, F.J. Dahmen, H. Holzel, and A. Meir, *Spectrochim. Acta* **30B** 449 (1975).

40 R. Nakashima, S. Sasaki, and S. Shibata, *Anal. Chim. Acta* **70**, 265 (1974).

41 M. Suzuki, *Buseki Kagan*, **17**, 1529 (1968).

42 M. Suzuki, *Buseki Kagan*, **19**, 207 (1970).

43 M. Suzuki, *Buseki Kagan*, **19**, 204 (1970).

44 D. Huang and M. Blades, *J. Anal. At. Spectrosc.*, **6**, 215 (1991).

45 H. Uchida, P.A. Johnson, and J.D. Winefordner, *J. Anal. At. Spectrosc.* **5**, 81 (1990).

46 A.H. Ali, K.C. Ng, and J.D. Winefordner, *J. Anal. At. Spectrosc.* **6**, 211 (1991).

47 Y.K. Zhang, S. Hanamura, and J.D. Winefordner, *Appl. Spectrosc.*, **39**, 226 (1985).

48 B.M. Patel, J.P. Deavor, and J.D. Winefordner, *Talanta*, **35**, 641 (1988).

49 J.D. Hwang, W. Masamba, B.W. Smith, and J.D. Winefordner, *Can. J. Spectrosc.*, **33**, 156 (1988).

50 P.A. Rizzi, *Microwave Engineering Passive Circuits*, Prentice-Hall, Englewood Cliffs, NJ (1988).

51 J.L. Altman, *Microwave Circuits*, Van Nostrand, Princeton, NJ (1964).

52 R.S. Alger, *Electron Paramagnetic Resonance: Techniques and Applications*, Interscience, New York (1968).

53 V.F. Verley, *Modern Microwave Technology*, Prentice-Hall, Englewood Cliffs, NJ (1987).

54 W. Sinnema, *Electronic Transition Technology, Lines, Waves and Antennas*, 2nd ed. Prentice-Hall, Englewood Cliffs, NJ (1988).

55 S.Y. Liao, *Microwave Devices and Circuits*, Prentice Hall, Englewood Cliffs, NJ (1980)

56 S. Chan and A. Montaser, *Spectrochim. Acta* **40B**, 1467 (1985).

57 M.H. Abdalla and J.M. Mermet, *Spectrochim. Acta* **37B**, 391 (1982).

58 K. Wolnik, D. Miller, C. Seliskar, and F. Fickey, *Appl. Spectrosc.* **39**, 930 (1985).

59 C. Seliskar and D. Warner, *Appl. Spectrosc.* **39**, 181 (1985).

60 P. Fleitz and C. Seliskar, *Appl. Spectrosc.* **41**, 679 (1987).

61 D. Miller, C. Seliskar, and T. Davidson, *Appl. Spectrosc.* **39**, 13 (1985).

62 D. Miller, H. Fannin, P. Fleitz, and C. Seliskar, *Appl. Spectrosc.* **40**, 611 (1986).

63 S. Chan, R. Van Hoven, and A. Montaser, *Anal. Chem.* **58**, 2342 (1986).

64 S. Hanamura, B.W. Smith, and J.D. Winefordner, *Can. J. Spectrosc.* **29**, 13 (1984).

65 H. Uchida, W.R. Masamba, T. Uchida, B.W. Smith, and J.D. Winefordner, *Appl. Spectrosc.* **43**, 425 (1989).

66 A.H. Ali, *Electrode Heating and Sample Vaporization in Capacitively Coupled Microwave Plasma Atomic Emission Spectrometry*, Ph.D. Dissertation, University of Florida, Gainesville (1991).

67 F.L. Grove, *Analytical Emission Spectroscopy*, Part II, Dekker, New York (1972).

68 W. Lotche-Holtgreven, *Evaluation of Plasma Parameters*, Ch. 3 in *Plasma Diagnostics*, W. Lotche-Holtgreven, Ed., North Holland Publishing Company, Amsterdam (1968).

69 T. Hasegawa and H. Haraguchi, *Fundamental Properties of Inductively Coupled Plasmas,* Ch. 8 in *Inductively Coupled Plasmas in Analytical Atomic Spectrometry*, A. Montaser and D.W. Golightly, Eds., VCH Publishers (1987).

70 K. Fallgatter, *Physical and Analytical Properties of a Microwave Excited Plasma*, Ph.D. Dissertation, University of Florida, Gainesville (1970).

71 H.R. Griem, *Spectral Line Broadening by Plasmas*, Academic Press, New York (1974).

72 M.W. Blades, and B.L. Caughlin, *Spectrochim. Acta* **40B**, 579 (1985).

73 M.C.E. Huber and W.H. Parkinson, *Astrophysics J.* **172**, 229 (1972).

74 J.M. Bridges and R.L. Kornblith, *Astrophysics J.* **192**, 793 (1974).

75 D.E. Blackwell, A.D. Petford, M.J. Shallis, and G.J. Simmons, *Mon. Not. R. Astron. Soc.* **191**, 445 (1980).

76 W.L. Wiese and G.A. Marlin, *Wavelengths and Transition Probabilities for Atoms and Atomic Ions, Part II, Transition Probabilities,* **NSRDS-NBS 68**, U.S. Government Printing Office, Washington, DC. (1980).

77 J. Mermet, *Spectroscopic Diagnostics: Basic Concepts* Ch. 10 in *Inductively Coupled Plasma Emission Spectroscopy-Part 2 Applications and Fundamentals.* P.W.J.M. Boumans, Ed., John Wiley and Sons, New York (1987).

78 J.M. Workman, P.G. Brown, D.C. Miller, C.J. Seliskar, and J.A. Caruso, *Appl. Spectrosc.* **40**, 857 (1986).

79 K. Tanabe, H. Haraguchi, and K. Fuwa, *Spectrochim. Acta* **38B**, 49 (1983).

80 Gy. Heltai, J.A.C. Broekaert, F. Leis, and G. Tolg, *Spectrochim. Acta* **45B,** 301 (1990).

81 J.M. Workman, P.A. Fleitz, H.B. Fannin, J.A. Caruso, and C.J. Seliskar, *Appl. Spectrosc.* **42**, 96 (1988).

82 P.G. Brown, J.M. Workman, D.L. Haas, P.A. Feitz, D.C. Miller, C.J. Seliskar, and J.A. Caruso, **40**, *Appl. Spectrosc.* **40,** 477 (1986).

83 J.F. Alder, R.M. Bombelka, and G.F. Kirkbright, *Spectrochim. Acta* **35B**, 163 (1980).

84 Y.Q. Tang and C. Trassy, *Spectrochim. Acta* **41B**, 143 (1986).

85 S.R. Goode, N.P. Buddin, B. Chambers, K.W. Baughman, and J.P. Deaver, *Spectrochim. Acta* **40B**, 317 (1985).

86 P.G. Brown, T.J. Brotherton, J.M. Workman, and J.A. Caruso, *Appl. Spectrosc.* **41**, 774 (1987).

87 M.H. Abdalla, and J.M. Mermet, *Spectrochim. Acta* **37B**, 391 (1982).

88 I. Ishii, H. Tan, S. Chan and A. Montaser, *Spectrochim. Acta*, **46B**, 901 (1991).

89 T.B. Reed, *Adv. High Temp. Chem.* **1**, 284 (1967).

90 S. Greenfield and H. McGeachin, *Anal. Chim. Acta*, **100**, 101 (1978).

91 S. Greenfield, I.L. Jones, and H. McGeachin, *Anal. Chim. Acta*, **74**, 225 (1975).

92 A. Montaser and J. Mortazavi, *Anal. Chem.* **52**, 255 (1980).

93 A.J. McCormack, S.C. Tong, and W.D. Cooke, *Anal. Chem.*, **37**, 1470 (1965).

94 C.A. Bache and D.L. Liske, *Anal. Chem.*, **37**, 1477 (1965).

95 W. Braun, N.C. Peterson, A.M. Baas, and M.J. Kuryko, *J. Chromatogr.* **55**, 237 (1971).

96 W.R. McLean, D.L. Stantan, and G.E. Penteth, *Analyst* **98**, 432 (1971).

97 D.F. Hagen, J. Belisle, and J.S. Markevka, *Spectrochim. Acta* **38B**, 377 (1983).

98 J.P.J. van Dalen, P.A. de Lezenne Conlander, and L. de Galan, *Anal. Chim Acta* **94**, 1 (1977).

99 F.A. Serravallo and T.H. Risby, *Anal. Chem.* **47**, 2141 (1975).

100 S.A. Estes, P.C. Uden, and R.M. Barnes, *Anal. Chem.* **53**, 1829 (1981).

101 C.J.M. Beenaker, P.W.J. Boumans, and P.J. Phillips, *Tech. Rev.* **39**, 65 (1980).

102 J.C. Bailar, Jr., H.J. Emelens, R. Nyholm, and A.F. Trontman-Dickenson, *Comprehensive Inorganic Chemistry*, Vol. 1, Pergamon Press, Oxford (1973).

103 R. R. Nakashima, *Bunseki Kigaku* **25**, 869 (1976).

104 I. Atsuya and K. Akatsuka, *Spectrochim. Acta* **36B**, 747 (1981).

105 H. Uchida, P.A. Johnson, and J.D. Winefordner, *J. Anal. At. Spectrom.* **5**, 81 (1990).

106 T. Nakahara, *Prog. Anal. Atom. Spectrosc.* **6**, 163 (1983).

107 W.B. Robbins and J.A. Caruso, *Anal. Chem.* **51**, 889A (1979).

108 A.E. Greenberg, R. Trussel, and L.S. Clesceri, Eds. *Selected Physical and Chemical Standard Methods for Students*. Port City Press, Baltimore (1986).

109 R. Bye, *Talanta* **29**, 797 (1982).

110 R.K. Winge, V.J. Peterson, and V.A. Fassel, *Appl. Spectrosc.*, **33**, 206 (1979).

111 C.T.J. Alkemade, *Anal. Chem.* **38**, 1252 (1966).

112 R. Hermann and C.T.J. Alkemade, *Chemical Analysis by Flame Photometry*. Interscience, New York (1963).

113 S. Fukishima, *Microchim. Acta* 596 (1959).

114 I. Yofe, R. Avni and M. Stiller, *Anal. Chim. Acta* **28**, 331 (1963).

115 P.B. Adams and W.O. Passmore, *Anal. Chem.* **38**, 630 (1966).

116 R.H. Wendt and V.A. Fassel, *Anal. Chem.* **38**, 337 (1966).

117 G.R. Kornblum and L. De Galan, *Spectrochim. Acta* **32B**, 455 (1977).

118 E.E. Pickett and S.R. Koirtyohann, *Spectrochim. Acta* **23B**, 235 (1968).

119 G.R. Kornblum and L. De Galan, *Spectrochim. Acta* **28B**, 139 (1973).

120 S.R. Koirtyohann, J.S. Jones, C.P. Jester, and D.A. Yates, *Spectrochim. Acta* **36B**, 49 (1981).

121 G.F. Larson, V.A. Fassel, R.H. Scott, and R.N. Kniseley, *Anal. Chem.* **47**, 238 (1975).

122 M.H. Abdalla, J.M. Mermet, and C. Trassy, *Anal. Chim. Acta* **87**, 329 (1976).

123 H. Kawaguchi, T. Ito, K. Ota, and A. Mizuike, *Spectrochim Acta*, **35B**, 199 (1980).

124 E.D Salin and G. Horlick, *Anal. Chem.* **51**, 2284 (1979).

125 D. Sommer and K. Ohls, *Frez. Z. Anal. Chem.* **304**, 97 (1980).

126 L. Blair and E.D. Salin, *Spectrochim. Acta* **47B**, 399 (1992).

127 V. Karanassios and G. Horlick, *Spectrochim. Acta Rev.* **13**, 89 (1990).

128 C.W. Mcleod, P.A. Clarke, and D.J. Mowthorpe, *Spectrochim. Acta* **41B** 63 (1986).

129 W.E. Pettit and G. Horlick, *Spectrochim. Acta* **41B**, 699 (1986).

130 Y. Shao and G. Horlick, *Appl. Spectrosc.* **40**, 386 (1986).

131 G. Zaray, J.A.C. Broekaert, and F. Leis, *Spectrochim. Acta* **43B**, 241 (1988).

132 L. Blain and E.D. Salin, *Spectrochim. Acta* **47B**, 205 (1992).

133 R. Guevremont and K.N. De Silva, Spectrochim. Acta **47B**, 371 (1992).

134 R. Guevremont and K.N. De Silva, Spectrochim. Acta **46B**, 67 (1991).

135 L. Ebdon and J.R. Wilkinson, *J. Anal. At. Spectrom.* **5**, 67 (1990).

136 N.Imai, *Anal. Chim. Acta* **235**, 381 (1990).

137 W. Shen, J.A. Caruso, F.C. Fricke, and R.D. Satzger, *J. Anal. At. Spectrom.* **5**, 451. (1990).

138 F.J. Langmyhr and G. Wibetoe, *Prog. Anal. At. Spectrom.* **8**, 193 (1985).

139 G. Zaray, P. Burba, J.A.C. Broekraet, and F. Leis, *Spectrochim. Acta* **43B**, 255 (1988).

140 V. Karanassios, M. Abdullah, and G. Horlick, *Spectrochim. Acta* **45B**, 119 (1990).

141 A. Lorber and Z. Goldbart, *Analyst* **110**, 155 (1985).

142 A.G. Page, K.H. Madraswala, S.V. Godbole, M.J. Kulkani, V.S. Mallapurkar, and B.D. Joshi, *Fres. Z. Anal. Chem.* **315**, 38 (1983).

143 D.C. Liang and M.W. Blades, *Spectrochim. Acta* **44B**, 1049 (1989).

144 M. Abdulla and H. Haraguchi, *Anal. Chem.* **57**, 2059 (1985).

145 A.G. Page, S.V. Godbole, K.H. Madraswala, M.J. Kulkarni, V.S. Mallapurkar, and B.D. Joshi, *Spectrochim. Acta* **39B**, 551 (1984).

146 Q. Jin, C. Zhu, M.W. Borer and G.M. Hieftje, *Spectrochim. Acta* **46B**, 417 (1991).

147 Y. Okamoto, M. Yasuda, and S. Murayama, *Jpn. J. Appl. Phys.* **29**, L670 (1990).

148 Y. Okamoto, *Anal. Sci.* **7**, 283 (1991).

BIOGRAPHICAL SKETCH

Wellington Riach Liamba Masamba of Chikaonda village, Machinga, Malawi, was born on April 10, 1960. He attended Balaka Secondary School from 1973 to 1977. He was admitted into the University of Malawi (Chancellor College) in 1977 where was awarded a Bachelor of Science degree with distinction in 1981 and a Bachelor of Science honors degree in 1982. In August of 1985 he entered the Graduate School at the University of Florida where he was awarded a masters degree in April, 1988. He continued on with the Ph.D. program at the University of Florida but took a two year break from 1989 to 1990.

I certify that I have read this study and that in my opinion it conforms to acceptable standards of scholarly presentation and is fully adequate, in scope and quality, as a dissertation for the degree of Doctor of Philosophy.

James D. Winefordner
James D. Winefordner, Chair
Graduate Research Professor of Chemistry

I certify that I have read this study and that in my opinion it conforms to acceptable standards of scholarly presentation and is fully adequate, in scope and quality, as a dissertation for the degree of Doctor of Philosophy.

Gerhard M. Schmid
Gerhard M. Schmid
Associate Professor of Chemistry

I certify that I have read this study and that in my opinion it conforms to acceptable standards of scholarly presentation and is fully adequate, in scope and quality, as a dissertation for the degree of Doctor of Philosophy.

Vaneica Y. Young
Vaneica Y. Young
Associate Professor of Chemistry

I certify that I have read this study and that in my opinion it conforms to acceptable standards of scholarly presentation and is fully adequate, in scope and quality, as a dissertation for the degree of Doctor of Philosophy.

Martin Vala
Martin T. Vala
Professor of Chemistry

I certify that I have read this study and that in my opinion it conforms to acceptable standards of scholarly presentation and is fully adequate, in scope and quality, as a dissertation for the degree of Doctor of Philosophy.

Eric R. Allen
Eric R. Allen
Professor of Environmental Engineering

This dissertation was submitted to the Graduate Faculty of the Department of Chemistry in the College of Liberal Arts and Sciences to the Graduate School and was accepted as partial fulfillment of the requirements for the degree of Doctor of Philosophy.

August 1992

Dean, Graduate School